Dalton Transactions

ROYAL SOCIETY OF CHEMISTRY

PAPER

View Article Online
View Journal | View Issue

Cite this: *Dalton Trans.*, 2020, **49**, 10185

Luminescent halogen-substituted 2-(*N*-arylimino) pyrrolyl boron complexes: the internal heavy-atom effect†

Ana I. Rodrigues, [a] Paramasivam Krishnamoorthy, [a,h] Clara S. B. Gomes, [a,i,j] Nicolas Carmona,[a] Roberto E. Di Paolo, [a] Piotr Pander, [c] João Pina, [d] J. Sérgio Seixas de Melo, [d] Fernando B. Dias, [c] Maria José Calhorda, [e] António L. Maçanita, [a,b] Jorge Morgado [f,g] and Pedro T. Gomes *[a,b]

A group of new boron complexes [$BPh_2\{\kappa^2N,N'$-NC_4H_3-2-C(H)=N-$C_6H_4X\}$] (X = 4-Cl **4c**, 4-Br **4d**, 4-I **4e**, 3-Br **4f**, 2-Br **4g**, 2-I **4h**) containing different halogens as substituents in the *N*-aryl ring have been synthesized and characterized in terms of their molecular properties. Their photophysical characteristics have been thoroughly studied in order to understand whether these complexes exhibit an internal heavy-atom effect. Phosphorescence emission was found for some of the synthesized halogen-substituted boron molecules, particularly for **4g** and **4h**. DFT and TDDFT calculations showed that the lower energy absorption band resulted from the HOMO to LUMO ($\pi-\pi^*$) transition, except for 2-I **4h**, where the HOMO–1 to LUMO transition was also involved. The strong participation of iodine orbitals in HOMO–1 is reflected in the calculated absorption spectra of the iodine derivatives, especially 2-I **4h**, when spin–orbit coupling (SOC) was included. Organic light-emitting diodes (OLEDs) based on these complexes, in the neat form or dispersed in a matrix, were also fabricated and tested. The devices based on films prepared by thermal vacuum deposition showed the best performance. When neat complexes were used, a maximum luminance (L_{max}) of 1812 cd m^{-2} was obtained, with a maximum external quantum efficiency (EQE_{max}) of 0.15%. An EQE_{max} of *ca.* 1% along with a maximum luminance of 494 cd m^{-2} were obtained for a device fabricated by co-deposition of the boron complex and a host compound (1,3-bis(*N*-carbazolyl)benzene, mCP).

Received 22nd May 2020,
Accepted 29th June 2020

DOI: 10.1039/d0dt01845g

rsc.li/dalton

1. Introduction

After the report of the first multi-layered organic-light emitting diodes (OLEDs), by Tang and Van Slyke,[1] many improvements have been achieved in this type of technology to the point of their being nowadays present in commercially available flat displays and lighting applications. In spite of this achievement, there is a continuous search for enhancements in this technology aiming to obtain better brightness, flexibility, stability and lower production costs.

In the production of luminescent emitters, there is already a variety of options based on fluorescent and/or phosphorescent chromophores, or in the newest thermally activated delayed fluorescent (TADF) molecules.[2] Tetracoordinate boron complexes containing bidentate *N*,*N*-; *N*,*O*-; *N*,*C*-; *C*,*C*-; *C*,*O*- and *O*,*O*- ligands gave rise to particularly interesting luminescent chromophores, some of them used in OLED devices with good electroluminescent properties.[3,4]

Our research group has already developed a reasonable number of tetracoordinate boron complexes bearing a 2-(*N*-

[a]*Centro de Química Estrutural, Instituto Superior Técnico, Universidade de Lisboa, Av. Rovisco Pais, 1049-001 Lisboa, Portugal.*
E-mail: pedro.t.gomes@tecnico.ulisboa.pt
[b]*Departamento de Engenharia Química, Instituto Superior Técnico, Universidade de Lisboa, Av. Rovisco Pais, 1049-001 Lisboa, Portugal*
[c]*Department of Physics, Durham University, South Road, Durham DH1 3LE, UK*
[d]*University of Coimbra, Coimbra Chemistry Centre, Department of Chemistry, Rua Larga, 3004-535 Coimbra, Portugal*
[e]*BioISI -Biosystems & Integrative Sciences Institute, Departamento de Química e Bioquímica, Faculdade de Ciências, Universidade de Lisboa, Campo Grande, Ed. C8, 1749-016 Lisboa, Portugal*
[f]*Instituto de Telecomunicações, Av. Rovisco Pais, 1049-001 Lisboa, Portugal*
[g]*Department of Bioengineering, Instituto Superior Técnico, Universidade de Lisboa, Av. Rovisco Pais, 1049-001 Lisboa, Portugal*
[h]*Centre for Environmental Research, Department of Chemistry, Kongu Engineering College, PerunduraiErode 638 060, India*
[i]*LAQV-REQUIMTE, Departamento de Química, Faculdade de Ciências e Tecnologia, Universidade NOVA de Lisboa, 2829-516 Caparica, Portugal*
[j]*UCIBIO-REQUIMTE, Departamento de Química, Faculdade de Ciências e Tecnologia, Universidade NOVA de Lisboa, 2829-516 Caparica, Portugal*

†Electronic supplementary information (ESI) available. Several subsections, also including CCDC 2004594–2004596. For ESI and crystallographic data in CIF or other electronic format see DOI: 10.1039/D0DT01845G

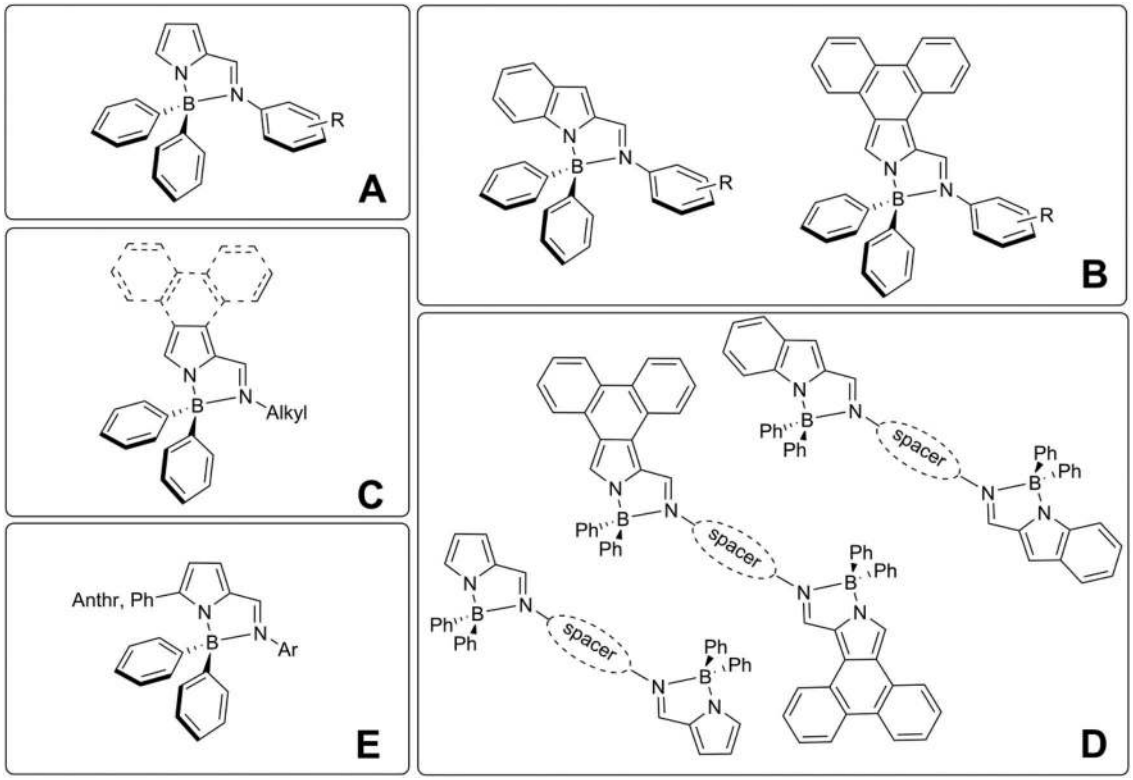

Chart 1 2-(*N*-arylformimino)pyrrolyl–BPh_2 complexes previously reported by our research group.

arylformimino)pyrrolyl ligand. Their emission colour could be tuned by varying the structural and electronic features of this scaffold. The 2-iminopyrrolyl-BPh_2 complexes containing donor and acceptor groups in the *N*-phenyl fragment (*e.g.* H, 2,6-*i*Pr_2, OMe, CN, *etc.*) (Chart 1, **A**)[5] proved to be blue to bluish-green fluorescence emitters. The boron analogues bearing fused aromatic fragments onto the C4–C5 or the C3–C4 bonds (indolyl or phenanthropyrrolyl, respectively) (Chart 1, **B**) are other good examples. For instance, the phenanthropyrrolyl derivatives exhibited fluorescence quantum yields in the range of 37–61%.[6] Other derivatives such as 2-(imino) and 2-(iminophenanthro)pyrrolyl-BPh_2 containing *N*-alkyl groups (methyl, *n*-octyl, *i*-propyl, cyclohexyl, *t*-butyl and adamantyl) were also reported as violet-blue emitters (Chart 1, **C**).[7] OLED devices based on binuclear 2-iminopyrrolyl-BPh_2 derivatives (Chart 1, **D**) achieved a luminance maxima of 4400 cd m^{-2}.[5a,8] The substitution of the 2-iminopyrrolyl ring at position 5 with aromatic substituents, such as phenyl or anthracenyl (Anthr), originated a new family of 5-substituted 2-(*N*-arylformimino)pyrrolyl boron complexes. These green and blue fluorescent emitters (Chart 1, **E**) were applied in the emissive layers of OLED devices with various structures, showing external quantum efficiencies up to 2.75% along with luminances as high as 23 530 cd m^{-2}.[9]

Interestingly, in all the previous studies, the observation of triplet formation *via* intersystem crossing was only identified in a single case (for a molecule of the type **A** with R = 4-CN, see Chart 1).[5] We describe in the present work a set of new halogen-substituted 2-(*N*-arylformimino)pyrrolyl–BPh_2 complexes, which were designed to investigate the possible existence of an internal heavy-atom effect,[10] promoting the triplet state formation *via* a spin–orbit coupling mechanism, namely for the heavier substituents. The photophysical properties of the new boron derivatives were thoroughly studied in order to conclude about the origin of light emission in these compounds. In addition, the new halogen-substituted 2-(*N*-arylimino)pyrrolyl boron complexes were characterized by NMR spectroscopy, elemental analysis and single crystal X-ray diffraction. DFT and TDDFT studies complemented the work by providing the geometry of the ground state, the singlet and triplet first excited states, as well as the nature of the absorption bands and an understanding of the importance of spin–orbit coupling in the emission of the halogenated complexes. At a later stage, OLEDs based on these complexes as emissive materials were fabricated and their performance assessed.

2. Results and discussion

2.1 Synthesis and characterization of halogen-substituted 2-iminopyrrole ligand precursors and halogen-substituted 2-iminopyrrolyl boron complexes

The halogen-substituted 2-formiminopyrrole ligand precursors **3c–3h** were synthesized *via* a condensation reaction of 2-formylpyrrole **1** (ref. 11) with different anilines **2c–2h** containing halogen substituents. The mixtures were refluxed at *ca.* 130 °C,

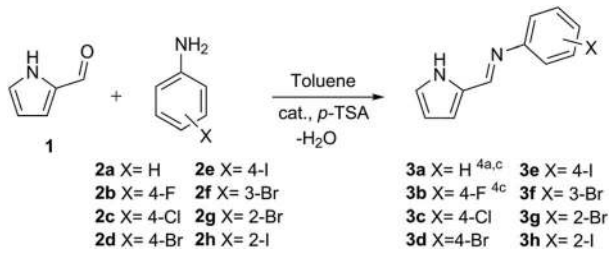

Scheme 1 Synthesis of halogen-substituted 2-(*N*-arylformimino) pyrrole ligand precursors **3c–3h**. The synthesis of compound **3c** was carried out in xylenes.

in toluene, with removal of water (Scheme 1), except in the case of **3c** that was refluxed in (a mixture of) xylenes.

The resulting ligand precursors **3c–3h** were obtained in moderate to high yields. Their molecular characterization was performed by NMR spectroscopy (^{1}H and ^{13}C) and elemental analysis. The 2-(*N*-arylformimino)pyrrole ligands **3a** and **3b** had already been reported by us[5a,c] and other research groups.[12] The syntheses of the *p*-chlorine, *p*-bromine, *p*-iodine, *m*-bromine and *o*-bromine derivatives **3c–3g**, although already reported in the literature,[12a,b,d,e,13] were carried out following the typical condensation procedure used in our group.[5–9,12f] The reaction of halogen-substituted 2-(*N*-arylformimino) pyrrole ligand precursors **3c–h** with triphenylboron under reflux, in toluene and under nitrogen, afforded the respective iminopyrrolyl boron complexes **4c–4h** in moderate to high yields (Scheme 2).

The final 2-(*N*-arylformimino)pyrrolyl–BPh_2 complexes **4c–4h**, containing halogen substituents at the *N*-phenyl ring, were molecularly characterized by different techniques, such as NMR spectroscopy (^{1}H, ^{13}C and ^{11}B), elemental analysis and single-crystal X-ray diffraction (complexes **4c**, **4d** and **4g**).

The formation of the four-coordinate boron complexes **4c–4h** is suggested by the absence of the N*H* proton resonance in the ^{1}H NMR and the appearance of a ^{11}B singlet in the range of δ 4.73–5.34 (three-coordinate ^{11}B resonances occur at higher fields in the region *ca.* 25 ppm).

The iminopyrrolyl boron complexes **4a** and **4b**, previously reported in the literature,[5] were included in this work as reference complexes, for comparison with complexes **4c–4h**.

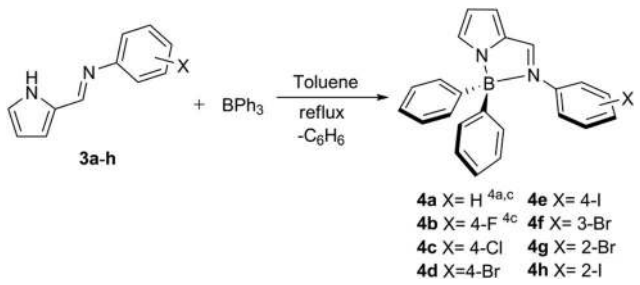

Scheme 2 Synthesis of 2-(*N*-arylformimino)pyrrolyl–BPh_2 complexes **4a–4h**.

2.2 X-ray diffraction studies

Single crystal X-ray diffraction structures were obtained for halogen-substituted 2-iminopyrrolyl–BPh_2 complexes **4c**, **4d** and **4g**. Fig. 1 presents the perspective views of their molecular structures. Crystallographic data for these complexes and the most significant bond distances and angles are listed in Table S1 and Fig. S1–S3 of the ESI,† respectively.

Molecules **4c** and **4d**, containing the substituent at the *p*-position of the aryl ring, far away from the BPh_2 and 2-iminopyrrolyl fragments, exhibit dihedral angles between the *N*-phenyl ring and the 2-iminopyrrolyl fragment of 45.19(16)° and −46.4(7)°, respectively, similar to that observed in **4a**.[5a,c] However, in these perspective views, it is clear that the *N*-phenyl core of the *o*-bromine complex **4g** appears to be approaching orthogonality relative to the 2-iminopyrrolyl fragment, with significantly higher dihedral angles of −69.4(3)°, 59.8(3)°, 72.0(3)°, and −70.4(3)°, for molecules A, B, C, and D, respectively (defined as C6–N2–C7–C8), owing to the high atomic radius of the bromine atom, exerting its bulkiness over the BPh_2 fragment.

The bite angles, corresponding to N1–B1–N2, have typical values of 94.91(12)° (**4c**), 94.8(4)° (**4d**) and 94.86(18)°, 94.88(18)°, 94.87(18)°, and 94.60(18)° (**4g**, molecules A, B, C, and D, respectively), consistent with modestly distorted tetrahedral geometries.

2.3 Photophysical studies

The photophysical properties of complexes **4c–4h** were studied in solution and in solid state and compared to complexes **4a** and **4b**. For solution studies, diluted THF solutions ($c < 2.7 \times 10^{-5}$ M) were prepared. In the case of solid state measurements, complexes **4c–4h** were mixed with ZEONEX and drop-cast on quartz or sapphire disks. The normalized absorption and emission spectra of the halogen-substituted iminopyrrolyl–BPh_2 complexes **4c–4h**, along with their emission colours, are presented in Fig. 2. No emission was found in the films of **4h** dispersed in ZEONEX.

The absorption wavelength maxima of complexes **4c–4h** in THF solution are within the 367–395 nm range (Table 1). Films of these complexes dispersed in ZEONEX show similar maxima (365–395 nm range), despite the small but significant decrease of the dielectric constant (ε = 7.6 in THF and 2.5 in ZEONEX). The molar extinction coefficients at the maximum wavelength (ε_{max}) in THF (Table 1) display values characteristic of 2-iminopyrrolyl–BPh_2 complexes, within the 1.5–2.8 × 10^4 L mol^{-1} cm^{-1} range, comparable to those of compounds **4a–4b** (1.7 and 1.9 × 10^4 L mol^{-1} cm^{-1}, respectively),[5] and of the similar complexes already published.[5–9]

The fluorescence quantum yield (Φ_f) values of complexes **4a–4g** in THF are within the 0.18–0.48 range, but for complex **4h** (the *N*-2-iodophenyl derivative), it is more than one order of magnitude lower (Φ_f = 0.01) and non-measurable in ZEONEX films. However, the moderately high molar singlet extinction coefficient of **4h** (ε_{max} = 1.5 × 10^4 L mol^{-1} cm^{-1}, Table 1) points to an allowed π–π* character of the lowest lying singlet

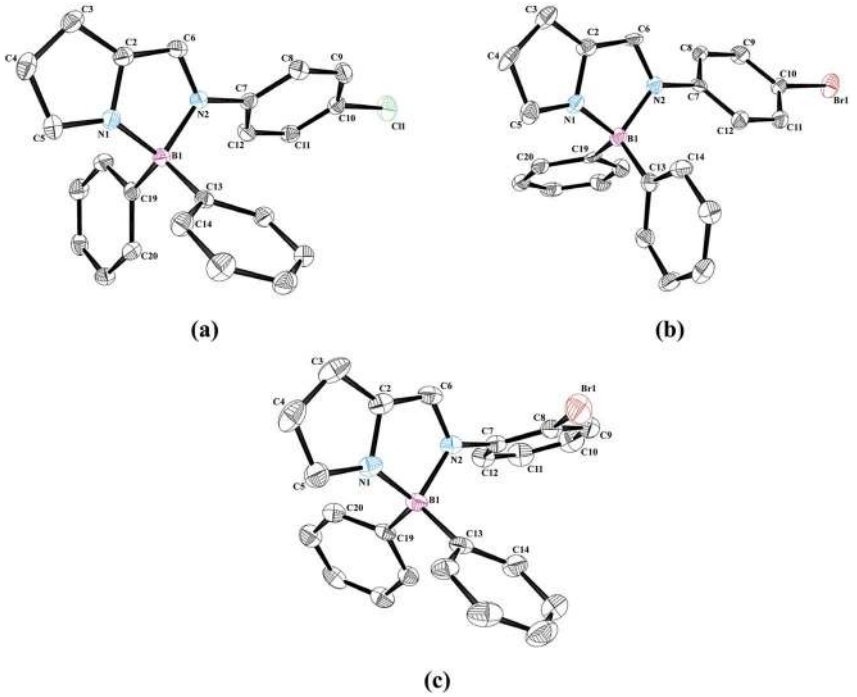

Fig. 1 Perspective views of the 2-iminopyrrolyl–BPh_2 complexes (a) **4c**, (b) **4d** and (c) **4g** (molecule A). The calculated hydrogen atoms were omitted for clarity and the ellipsoids were drawn at the 50% probability level.

excited state, similar to the other complexes. The increase of the Φ_f for the *p*-substituted *N*-phenyl complexes (0.25 up to 0.48, for *p*-F **4b** to *p*-I **4e**, respectively) indicates the absence of spin–orbit coupling when the heavy-atom is attached at the *para* position, because the increase of the halogen atom mass (F < Cl < Br < I) should increase the intersystem crossing rate constant (k_{isc}), thus decreasing the fluorescence quantum yield, $\Phi_f = k_f/(k_{ic} + k_{isc})$.

The fluorescence decays of complexes (**4a** to **4g**) in THF were single exponentials with fluorescence lifetimes (τ_f) around 2 ± 0.5 ns, from which the values of the fluorescence (k_f) and sum of the non-radiative rate ($k_{nr} = k_{ic} + k_{isc}$) constants were obtained (Table 1). The exception was the fluorescence decay of complex **4h** that required a sum of three exponential terms with decay times (τ_i) equal to 0.027, 0.16 and 2.27 ns and pre-exponential coefficients (A_i) equal to 0.62, 0.30 and 0.08, respectively, to be properly fitted (Fig. S4, in ESI†). This complexity indicates the presence of a fast additional excited-state process (a photoreaction), responsible for the extremely small fluorescence quantum yield of **4h** ($\Phi_f = 0.01$). Briefly, the two shortest decay times are assigned to the quenched fluorescence decay of **4h** and the longest time to the emission of a photoproduct (see detailed Discussion in the ESI†). In order to evaluate approximate values for the fluorescence (k_f) and the sum of the non-radiative (k_{nr}) constants, the quenched lifetime of **4h** was assumed equal to the average time of the two shortest decay times ($\tau_{average} = \Sigma A_i\tau_i^2/\Sigma A_i\tau_i = 0.13$ ns).

The k_f values of complexes **4a–4f** in THF are similar (within the 0.14–0.19 ns^{-1} range), decreasing to 0.09 and 0.08 ns^{-1} for the *ortho*-substituted complexes **4g** and **4h**. This diminution is confirmed by TDDFT calculations (see Table 3 and the following Discussion in Section 2.4).

The non-radiative rate constant (k_{nr}) values are within the 0.35 ± 0.14 ns^{-1} range except for complex **4h** whose k_{nr} value (7.66 ns^{-1}) is 20-fold larger than those of the other complexes, consistent with the presence of the additional non-radiative process indicated by the multi-exponential fluorescence decay.

In ZEONEX films, the photoluminescence rate constants (k_{PL}) are similar to those in THF, but the non-radiative rate constants are lower, explaining the higher values of the photoluminescence quantum yields (Φ_{PL}) in ZEONEX.

In order to split the non-radiative rate constants (k_{nr}) of the new complexes (**4c** to **4h**) into their internal conversion (k_{ic}) and intersystem crossing (k_{isc}) rate constants, the triplet formation quantum yields (Φ_T) and the triplet lifetimes (τ_T) were also measured, using nanosecond-laser flash photolysis. The transient absorption spectra of complexes **4c–4g** decayed single-exponentially with lifetimes (τ_T) within the 35–51 μs range (Table 2). Complex **4h** was again the exception, with decays at λ_{abs} < 440 nm generally requiring sums of two exponential terms plus a constant to be properly fitted, which indicates the presence of other absorbing species besides the triplet. For longer wavelengths (λ_{abs} = 450 nm), where only $T_1 \rightarrow T_n$ transitions are expected, acceptable fits with single exponentials plus a constant ($A_{abs} = a \times \exp(-t/\tau_T) + b$) were obtained with values of τ_T = 28 μs, a = 0.67 and b = 0.33 (Fig. S5, ESI†). The triplet lifetime τ_T = 28 μs (Table 2), is slightly shorter than that of **4g** (35 μs), as expected from the

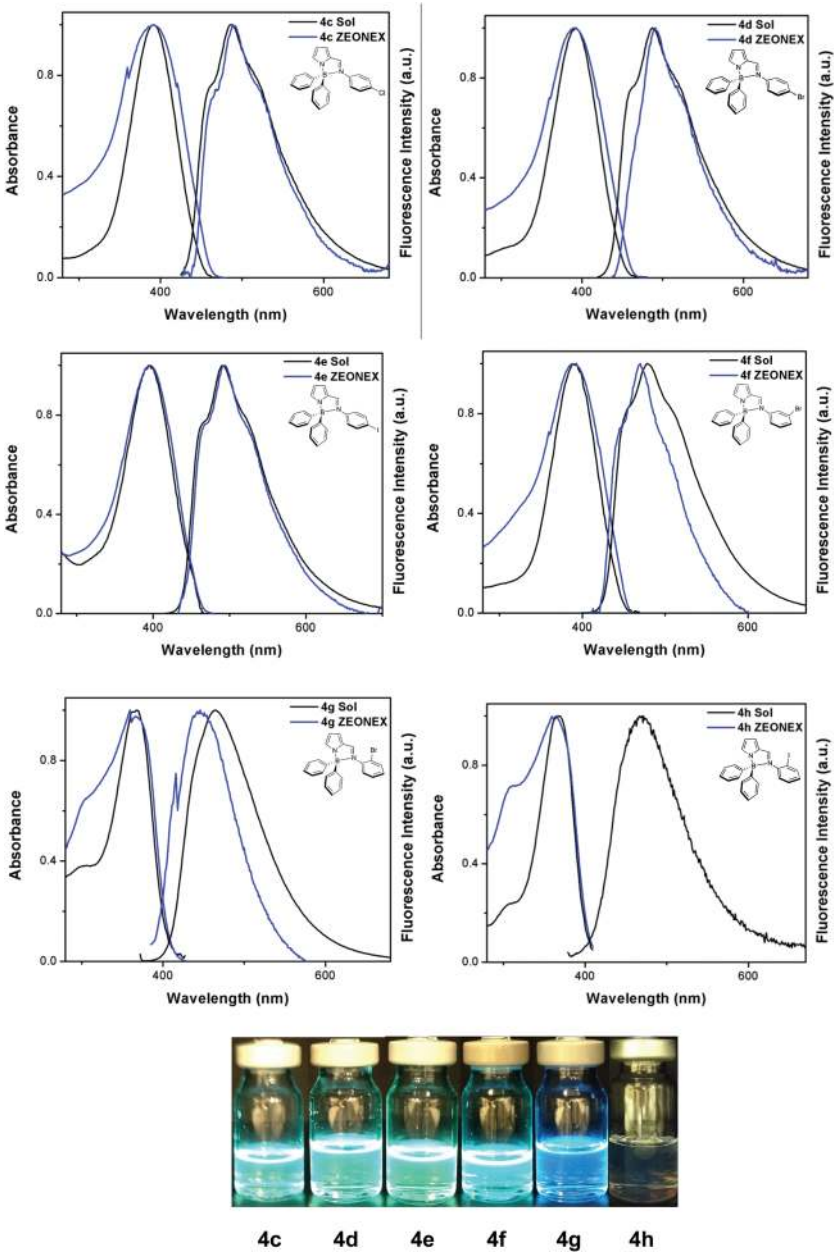

Fig. 2 Normalized absorption and emission spectra of complexes **4c–4h** in solution (THF) and ZEONEX film, at 293 K. Colours of the respective complexes in THF solution, under UV-irradiation at 365 nm, are also presented (bottom).

larger spin–orbit coupling effect on the $T_1 \rightarrow S_0$ transition. The significant value of b (0.33) is consistent with the absorption of ground-state species resulting from the photoreaction of **4h**. The results (Φ_T, $k_{isc} = \Phi_T/\tau_f$ and $k_{ic} = k_{nr} - k_{isc}$) are shown in Table 2.

The k_{isc} values are small (≈0 to 0.03 ns^{-1}) for the *para*-substituted **4c–4e** series, slightly increase for the *m*-substituted **4f** (0.05 ns^{-1}) and clearly increase for the *ortho*-substituted compounds **4g** and **4h** (0.11 and 0.39 ns^{-1}), indicating that spin–orbit coupling is most efficient when the heavy-atom is bonded at the *ortho* position. Actually, **4h** is the only compound where the introduction of the spin–orbit coupling in the calculations induces significant changes in the calculated absorption spectrum (see below Section 2.4).

The k_{ic} values of compounds **4c–4g** are within the 0.25 ± 0.06 ns^{-1} range, with the k_{ic} value of **4h** (7.27 ns^{-1}) being much larger than those of the other compounds, as expected. This means that, in the case of **4h**, $k_{nr} = k_{isc} + k_{ic} + k_{reaction}$.

The photoreactivity of **4h** may be due to the contribution of the p(I) → π*(iminopyrrolyl) transition for the S_1 state leading to some charge transfer from the iodine p-orbitals (HOMO−1) to the LUMO orbital, essentially located on the iminopyrrolyl moiety (see Fig. 5 and following discussion in Computational studies). Actually, homolytic photodissociation of iodine has

Table 1 Wavelength maximum (λ_{abs}^{max}) and molar extinction coefficient (ε_{max}) of the absorption band, wavelength maximum (λ_{em}^{max}), fluorescence quantum yields (Φ_f and Φ_{PL}), fluorescence lifetimes (τ_f and τ_{PL}), radiative rate constants (k_f and k_{PL}) and sum of non-radiative rate constants (k_{nr}) in solution (THF) and in solid state (ZEONEX 480 film), respectively, of boron complexes **4a–4h**, at 293 K

		Solution (THF)							Solid state (ZEONEX 480 film)					
Complex	X	λ_{abs}^{max} (nm)	ε_{max} [a]	λ_{em}^{max} (nm)	Φ_f	τ_f [b] (ns)	k_f [c] (ns^{-1})	k_{nr} [d] (ns^{-1})	λ_{abs}^{max} (nm)	λ_{em}^{max} (nm)	Φ_{PL}	τ_{PL} (ns)	k_{PL} [e] (ns^{-1})	k_{nr} [f] (ns^{-1})
4a	None[g]	383	1.7	479	0.34	1.9	0.18	0.35	[h]	[h]	[h]	[h]	[h]	[h]
4b	4-F[g]	381	1.9	478	0.25	1.5	0.16	0.49	[h]	[h]	[h]	[h]	[h]	[h]
4c	4-Cl	391	2.2	487	0.30	2.1	0.14	0.33	391	490	0.66	4.0	0.17	0.09
4d	4-Br	393	1.7	487	0.38	2.4	0.16	0.26	390	491	0.62	3.9	0.16	0.10
4e	4-I	395	2.8	492	0.48	2.5	0.19	0.21	395	494	0.53	3.5	0.15	0.13
4f	3-Br	389	1.8	478	0.37	2.6	0.14	0.24	387	470	0.59	3.8	0.16	0.11
4g	2-Br	367	1.7	464	0.18	2.0	0.09	0.42	367	445	0.31	2.7	0.11	0.26
4h	2-I	369	1.5	470	0.01	0.13[i]	0.08	7.66	365	[j]	[j]	[j]	[j]	[j]

[a] 10^4 L mol^{-1} cm^{-1}. [b] From single exponential decays. [c] $k_f = \Phi_f/\tau_f$. [d] $k_{nr} = (1 - \Phi_f)/\tau_f$. [e] $k_{PL} = \Phi_{PL}/\tau_{PL}$. [f] $k_{nr} = (1 - \Phi_{PL})/\tau_{PL}$. [g] Ref. 5. [h] Not available. [i] Average decay time from two exponential terms. [j] Non-emissive.

Table 2 Fluorescence lifetime (τ_f), radiative rate constant (k_f), sum of non-radiative rate constants (k_{nr}), triplet formation quantum yield (Φ_T), triplet lifetime (τ_T), intersystem crossing rate constant (k_{isc}) and internal conversion rate constant (k_{ic}), of boron complexes **4c–4h**, in THF, at 293 K

Complex	X	τ_f [a] (ns)	k_f [b] (ns^{-1})	k_{nr} [c] (ns^{-1})	Φ_T	τ_T (μs)	k_{isc} [d] (ns^{-1})	k_{ic} [e] (ns^{-1})
4c	4-Cl	2.1	0.14	0.33	[f]	[f]	[f]	[f]
4d	4-Br	2.4	0.16	0.26	0.04	51	0.02	0.25
4e	4-I	2.5	0.19	0.21	0.08	37	0.03	0.18
4f	3-Br	2.6	0.14	0.24	0.14	54	0.05	0.19
4g	2-Br	2.0	0.09	0.42	0.21	35	0.11	0.31
4h	2-I	0.13[g]	0.08	7.66	0.05	28	0.39	7.27[h]

[a] From single exponential decays. [b] $k_f = \Phi_f/\tau_f$. [c] $k_{nr} = (1 - \Phi_f)/\tau_f$. [d] $k_{isc} = \Phi_T/\tau_f$. [e] $k_{ic} = k_{nr} - k_{isc}$. [f] No signal was observed that could be attributed to the triplet state absorption. [g] Average decay time from two exponential terms. [h] Value of $k_{ic} + k_{reaction}$.

been observed for iodine-substituted aromatic rings or other chromophores.[14] In the case of **4h**, the reaction is described by two fast decay times, which is consistent with reversible homolytic cleavage of the iodine-C bond followed by a separation of the resulting radicals (see the ESI†). Complete elucidation would require further photochemical studies that are beyond the purpose of this work.

Fig. 3 compares the emission spectra of diluted solutions of complexes **4e–4h** in 2-MeTHF glasses, at 77 K, measured at two different delay times after excitation: Δt = 0 ms, to collect all luminescence (fluorescence and phosphorescence), and Δt = 0.05 ms, with most of the fluorescence being gated-out and exclusively collecting phosphorescence.

Phosphorescence emission at Δt = 0.05 ms was not detected for complex **4c**, being very weak for complexes **4d**, **4e** and **4f** (close to the background noise). For complexes **4g** and **4h**, the *ortho*-substituted bromine and iodine compounds, phosphorescence was clearly observed, indicating that the internal heavy-atom effect is the highest in these two compounds, as mentioned before. The smaller phosphorescence emission intensity of **4h** relative to **4g** results from the concurrent photoreaction of **4h**, leading to a four-fold smaller Φ_T (Table 2). It is worth noting that at Δt = 0 ms the phosphorescence intensity of complex **4h** competes with that of fluorescence and complex **4g** shows residual phosphorescence peaking at 518 nm and 561 nm.

2.4 Computational studies

The ground state geometry of all the complexes was obtained from DFT calculations (ADF program) using the PBE0 functional, with a TZP basis set for all atoms, considering spin–orbit coupling (SOPERT) and the effect of the THF solvent (method A). Calculations were also performed with the B3LYP functional (method B) and, in both cases, using a D3 Grimme correction (methods A/D3 and B/D3, more in Computational details). TDDFT calculations were used to determine the geometry of the first singlet and triplet excited states. The geometries obtained for complexes **4a–4h** are shown in Fig. 4. Although geometries for **4a** and **4b** have been published,[5] they had not been calculated in these conditions for **4b** (method A)[5c] and had not been reported in detail for **4a**.[9]

In the ground state, the relevant dihedral angle C6–N2–C7–C8 in the 2-iminopyrrolyl ligand varies between 35° and 39° (or −36° and −38°) for the complexes without substituents (**4a**) and with substituents in positions 3 and 4 (**4c–f**). The two complexes **4g** and **4h**, with *ortho* substituents, display a much higher angle (58 and 59°, respectively), owing to steric repulsion with the pyrrolyl group. These results agree in general with the values obtained for this angle by X-ray crystallography, namely 45.19(16)° for **4c**, −46.4(7)° for **4d**, and −69.4(3)°, 59.8(3)°, 72.0(3)°, and −70.4(3)°, for the four independent

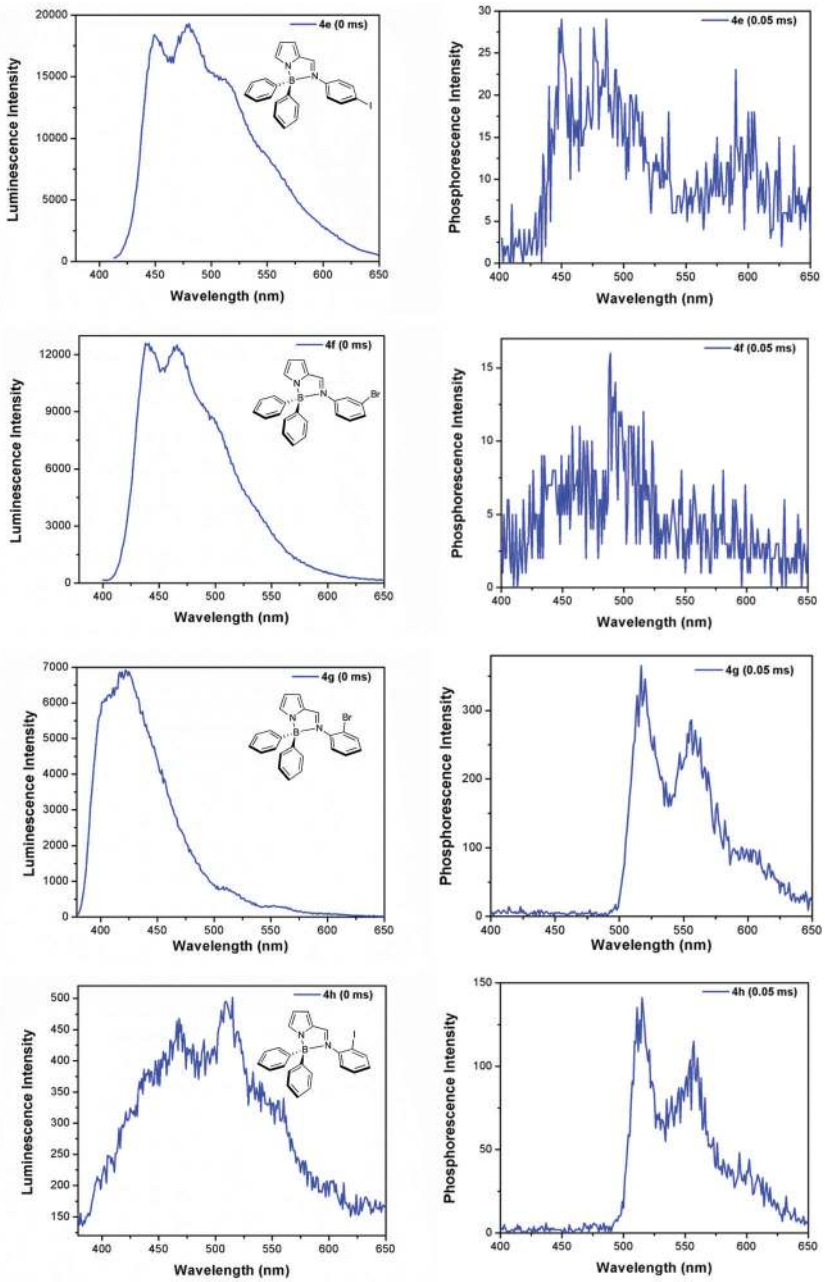

Fig. 3 Fluorescence and phosphorescence emission of complexes **4e–4h**, in 2-MeTHF, at 77 K, measured with a 10 ms sample window, at 0 (left) and 0.05 ms (right) delay times after excitation.

molecules of **4g**. The higher values in the solid can be assigned to the repulsion between adjacent molecules.

In both singlet and triplet excited states, the C6–N2–C7–C8 dihedral angle approaches zero for complexes **4a–f**. The other two complexes behave differently. While in the 2-Br derivative **4g**, the dihedral angle drops significantly from −59° to −29° in the singlet and −32° in the triplet, in the 2-I derivative **4h**, the dihedral angle increases from −58° to −66° in the singlet, but drops to −32° in the triplet. These values are very similar to those obtained by the other approaches referred above[9] and the one we used in earlier publications,[5] as shown in Table S2.†

TDDFT calculations were used to calculate the absorption spectrum of all the complexes (method A with a TZ2P basis set; results from other approaches are given in the ESI†). The absorption maxima for all the complexes are given in Table 3.

The calculated values are higher than the experimental ones, but they reflect the trends, namely the significantly higher absorption energies for **4g** and **4h**. The lowest energy absorption band results for all complexes, except for **4h**, from a HOMO to LUMO transition in the following percentage (oscillator strength): **4a** 96.2 (1.05), **4b** 95.9 (0.98), **4c** 96.3 (1.11), **4d** 96.5 (1.14), **4e** 96.7 (1.19), **4f** 95.8 (1.03), **4g** 92.0%

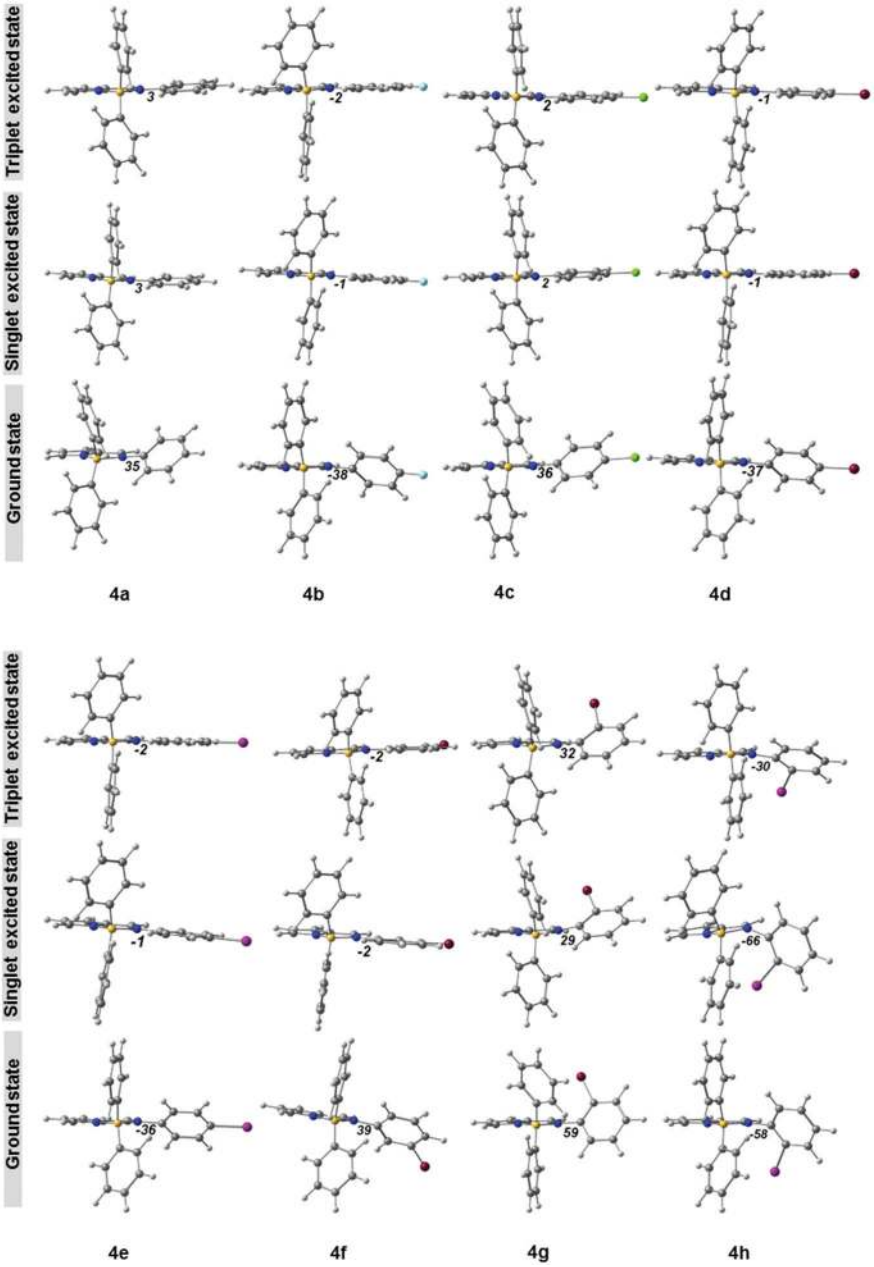

Fig. 4 Calculated geometries of the ground state (DFT) and of the first singlet and triplet excited states (TDDFT) of complexes **4a–4h**; the numbers represent the C6–N2–C7–C8 dihedral angle (°) for each species.

(0.78). The same band for complex **4h** arises from a HOMO to LUMO (87%) and a HOMO−1 to LUMO (8%) transition, with an oscillator strength of 0.65.

The HOMOs and LUMOs of **4a–4h** and HOMO−1 of **4h** are shown in Fig. 5, with their energies (see also Table S3†). It is very clear that the energies are almost exactly the same for the 4-substituted complexes (**4b–4e**), with the LUMOs being slightly destabilized and the HOMOs stabilized for the 2-substitued ones (**4g–4h**), while 3-Br (**4f**) only exhibits the stabilization of the HOMO. The HOMOs and LUMOs are localized in the iminopyrrolyl for **4a–4g**, with a very small participation of the halogen in both HOMO and LUMO (4-F), or in the HOMO (4-Cl, Br, I), with the contribution of the halogen increasing from F to I. The transition can be assigned as an intraligand (IL) $\pi \rightarrow \pi^*$ (iminopyrrolyl) with a small (**4b–4e**) or no (**4g**) participation of the halogen.

The orbitals of **4h** are different, since the contribution of the iminopyrrolyl ligand practically does not include the *N*-phenyl substituent, both in the HOMO and LUMO. The HOMO−1, however, is localized in two phenyls (on the iminopyrrolyl and on the boron), as well as in iodine, being C–I π-antibonding. In this complex the transition is essentially $\pi \rightarrow \pi^*$ (iminopyrrolyl) with some p(I) $\rightarrow \pi^*$ (iminopyrrolyl) charge transfer character.

Table 3 Calculated (method A) and experimental transition energy maxima (eV) of the lowest energy absorption band (E_{abs}^{max}), of the emission band (E_{em}^{max}), and calculated and experimental fluorescence rate constants (k_f) of boron complexes **4a–4h** in solution

		E_{abs}^{max} (eV)		E_{em}^{max} (eV)		k_f (ns^{-1})	
Complex	X	Calc.	Exp.	Calc.	Exp.	Calc.[a]	Exp.
4a	None	3.45	3.24[a]	2.73	2.59[a]	0.54	0.18[b]
4b	4-F	3.62	3.25[a]	2.67	2.59[a]	0.56	0.16[b]
4c	4-Cl	3.53	3.17	2.66	2.55	0.60	0.14
4d	4-Br	3.53	3.16	2.65	2.55	0.62	0.16
4e	4-I	3.50	3.14	2.61	2.52	0.62	0.19
4f	3-Br	3.61	3.19	2.76	2.59	0.58	0.14
4g	2-Br	3.82	3.38	2.83	2.67	0.49	0.09
4h	2-I	3.75	3.36	2.54	2.64	0.36	0.08

[a] k_f(calc.) = 1/τ(calc.), ref. 5. [b] Values from ref. 5.

The calculated fluorescence rate constants (k_f) are higher than the experimental ones, but they follow the main trend, with the values for **4g** and **4h** being the smallest. Since the calculations included spin orbit coupling (SOC), it was possible to analyse its role. It can be seen by the percentage of triplet states contributing to the absorption bands and the position of the maxima. In almost all complexes, the first excited state is ~100% singlet (for instance, the number for 4-Br (**4d**) is 99.5%) and there is no shift in the absorption maximum when the calculation is performed with SOC, and the same happens for the F, Cl, and Br derivatives. The situation changes for the iodine containing molecules. In **4e** (4-I), the first excited state is 99.3% singlet, and small amounts (<1%) of several triplet states, while the maximum shifts from 355 to 356 nm with SOC. The effect is more pronounced for **4h** (2-I), where the first excited state is 92.7% S_1, 3.6% T_1. The 2 nm shift of the absorption maximum is visible in Fig. 6 for **4h** (a similar picture is shown in Fig. S6, ESI,† for **4e**).

These features are in relatively good agreement with the experimental results described in the previous section, since the larger effect of spin–orbit coupling is observed in **4h** being much smaller in the second iodine derivative **4e**. The effect of bromine is not detected in the calculations, but it is also smaller in the emission features. We calculated the energy of the phosphorescence by optimizing with TDDFT the lowest triplet excited state. Table S4, ESI,† shows the calculated energies of singlet and triplet states of complexes **4a** to **4h** using various methods. For **4g**, the experimental triplet energy, E_T^{0-0}, is 2.39 eV (518 nm) (Fig. 3), while the calculated value is 1.89 eV (method A, Table S4 in ESI†). This is much lower than the experimental energy. The method had not been tested for the calculation of the energy of triplets, since this effect was not observed previously in this family.

A similar role played by iodine has been described for gallium and aluminium corrole complexes and their iodinated derivatives (three and four iodine atoms).[15] TDDFT calculations with and without spin–orbit coupling showed the participation

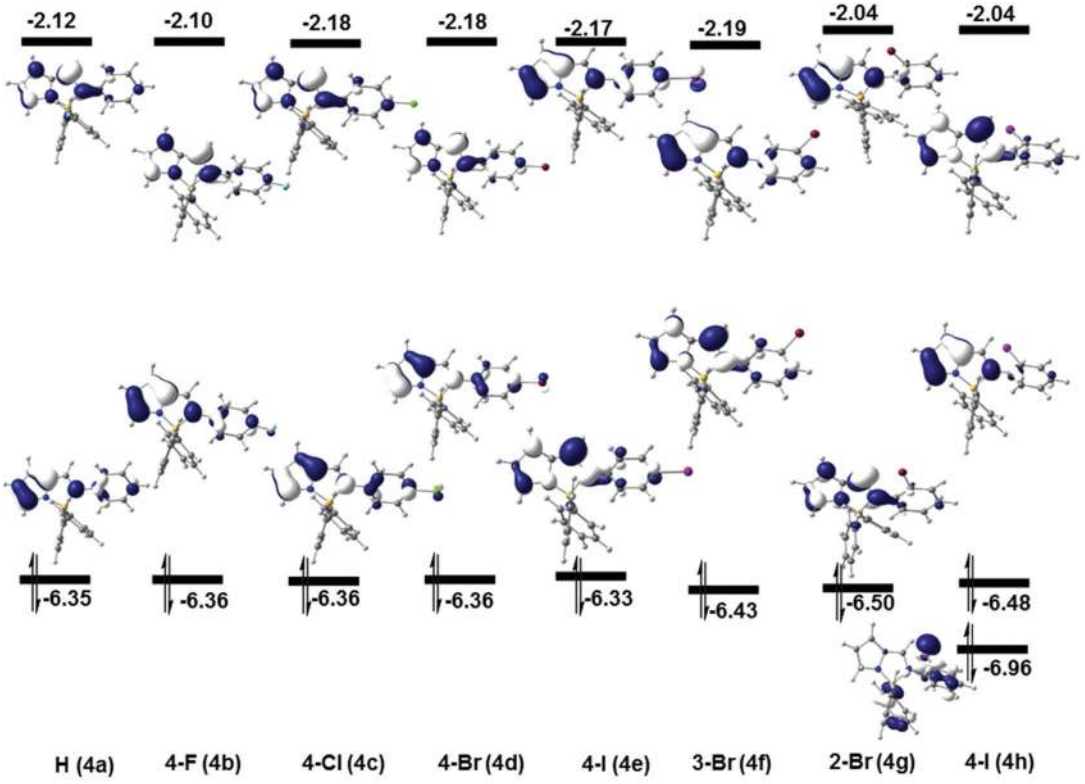

Fig. 5 Energies of the HOMOs and LUMOs of complexes **4a–4h** and HOMO–1 of **4h** with their 3D representation (the arrows indicate double occupation of the HOMOs).

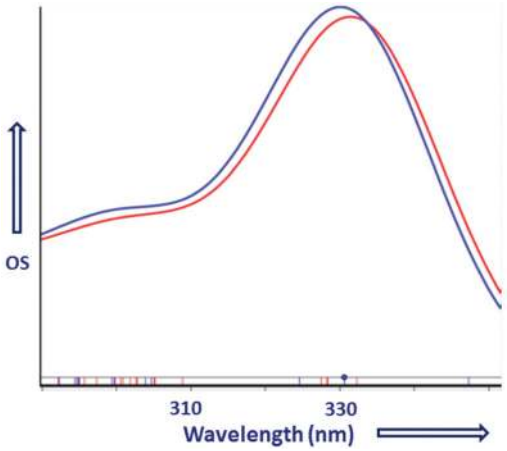

Fig. 6 Calculated absorption spectrum of complex **4h**: with SOC (red) and without SOC (blue).

of iodine in occupied orbitals, and its increase with the number of I atoms in the molecule, and reflected the strength of spin–orbit coupling. Despite the different nature of the absorption spectrum of these complexes, the charge transfer states from iodine to corrole parallel the charge transfer from iodine to iminopyrrolyl and the analogous role played by iodine.

2.5 Electrochemical properties

The new halogen-substituted complexes **4c–4h** and parent complexes **4a–4b** were characterized by cyclic voltammetry (CV) (Fig. S7–S12, ESI†). The measurements were carried out in tetrabutylammonium perchlorate/dichloromethane electrolyte solutions, at room temperature and under inert (N_2) atmosphere. The oxidation and reduction onset potentials were used to calculate the electron affinities (EA) and ionization potentials (IP), after conversion to the absolute scale with the Fc/Fc^+ (ferrocene/ferrocenium ion redox couple) as an external reference.[5a] As the energy level of Fc/Fc^+ (ferrocene/ferrocenium ion redox couple) is at 4.80 eV below the vacuum level, we calculated IP (eV) = $E_{onset,ox}$ (V) + (4.80 − E_{Fc/Fc^+}) and EA (eV) = $E_{onset,red}$ (V) + (4.80 − E_{Fc/Fc^+}), where E_{Fc/Fc^+} represents the measured half-wave potential of Fc/Fc^+. The values obtained are summarized in Table 4 along with the energies of the HOMOs and LUMOs of the corresponding complexes calculated by DFT with solvent correction (CH_2Cl_2).

The values of −IP show a correlation with the energies of the HOMOs, although with IP values differing between 0.08 and 0.26 eV from the calculated ones (see Fig. S13, ESI†). The −EA values also correlate with the calculated LUMO energies, with differences varying between 0.10 and 0.21 eV (see Fig. S13, ESI†).

2.6 Electroluminescence studies

The materials presented above (**4b–4h**) were tested as emissive materials in organic light-emitting diodes (OLEDs), with OLEDs based on complex **4h** failing to show any measurable emission. Thin films of the complexes were prepared by either spin-coating or vacuum thermal deposition. The performance of the full set of devices tested can be found in the ESI.†

Table 4 Ionization potentials (IP), electron affinities (EA) and IP–EA values of complexes **4a–4h**, estimated from cyclic voltammetry measurements, and corresponding energies of HOMOs and LUMOs determined by DFT (CH_2Cl_2). All values in eV

		Cyclic voltammetry			DFT (CH_2Cl_2)	
Complex	X	IP	EA	IP–EA	E_{HOMO}	E_{LUMO}
4a	None	5.64[a]	2.82[a]	2.82	−5.51	−2.98
4b	4-F	5.66[a]	2.86[a]	2.80	−5.49	−2.98
4c	4-Cl	5.70	2.81	2.89	−5.53	−2.99
4d	4-Br	5.67	2.85	2.82	−5.52	−2.99
4e	4-I	5.68	2.88	2.80	−5.49	−2.98
4f	3-Br	5.68	2.81	2.87	−5.60	−3.01
4g	2-Br	5.78	2.73	3.05	−5.62	−2.91
4h	2-I	5.86	2.70	3.16	−5.60	−2.91

[a] Values from ref. 5.

The best performing OLEDs were obtained when thin films of the boron complexes were prepared by vacuum thermal deposition.

Table 5 shows the performance parameters of a group of devices based on the films of complexes **4c**, **4d** and **4g** prepared by thermal vacuum deposition, with the structure: ITO (100 nm)/PEDOT:PSS (40 nm)/TPD (20 nm)/Complex (*ca.* 80 nm)/Bphen (11 nm)/LiF (1.5 nm)/Al (80 nm).

In this series, **4c**-based OLED showed the best performance, with a maximum luminance of 1812 cd m^{-2}, with an EQE of 0.15%. It is worth pointing out that for OLEDs based on all three complexes, **4c**, **4d** and **4g**, the maximum emission is red shifted with respect to PL emission of the corresponding sublimed films (Fig. S15 in the ESI†).

A multilayer OLED based on **4e** with the structure, ITO/HAT-CN (10 nm)/TAPC (25 nm)/mCP co 10% **4e** (25 nm)/TPBi (40 nm)/LiF (0.8 nm)/Al (100 nm) (Fig. 7(a)), was also prepared by vacuum thermal deposition.

Commercially available hexaazatriphenylenehexacarbonitrile (HAT-CN) was used as a hole injection layer and *N*,*N*-bis(4-methylphenyl)-benzenamine (TAPC) was used as a hole-transporting layer. 2,2′,2′-(1,3,5-Benzinetriyl)-tris(1-phenyl-1-benzimidazole) (TPBi) was selected as electron-transporting material, and lithium fluoride (LiF) as an electron injection layer with aluminium (Al) as the cathode. Complex **4e** was dis-

Table 5 Characteristics of OLED devices based on vacuum thermal deposited complexes **4c**, **4d** and **4g** including maximum luminance (L_{max}, cd m^{-2}), external quantum efficiency (EQE_{max}, %), current efficiency (η_L, cd A^{-1}), and Commission Internationale de l'Éclairage (CIE) colour coordinates

		ITO/PEDOT:PSS/TPD/Complex/Bphen/LiF/Al			
Complex	X	L_{max}	EQE_{max}	$\eta_{L,max}$	CIE
4c	4-Cl	1812	0.15	4.9×10^{-1}	0.30, 0.51
4d	4-Br	488	0.03	1.2×10^{-1}	0.33, 0.53
4g	2-Br	4	0.006	1.2×10^{-2}	0.29, 0.38

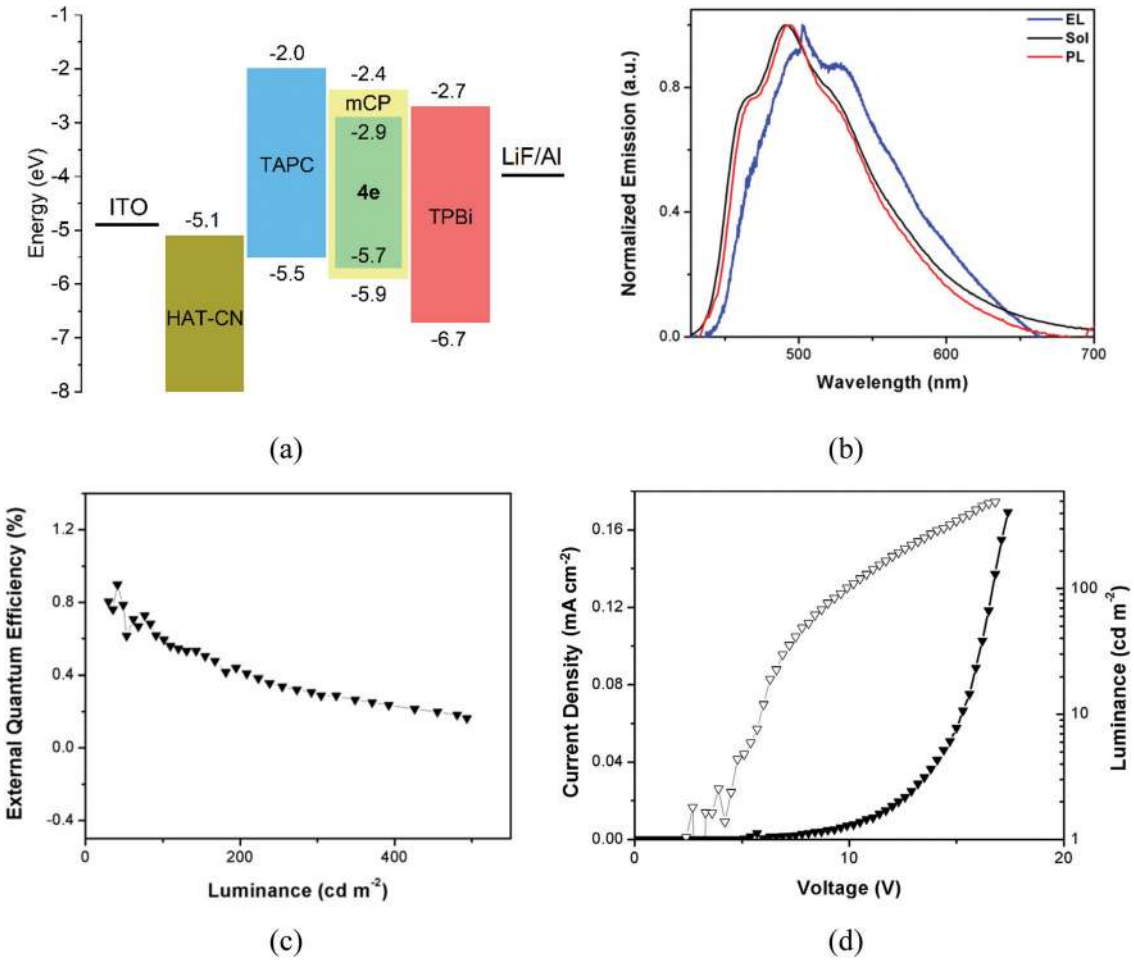

Fig. 7 Characteristics of the OLED device fabricated using complex **4e** as the emitter and mCP as host: (a) Schematic device energy level structure; (b) electroluminescence spectra (EL) compared with the film photoluminescence (PL) and solution fluorescence spectra in THF (Sol); (c) external quantum efficiency (EQE) *vs.* luminance; and (d) current density (filled symbols)/luminance (open symbols) *vs.* voltage.

persed in mCP (1,3-bis(*N*-carbazolyl)benzene) (10%), which was selected due to its energy levels: HOMO at −5.9 eV, below that of **4e** (considering E_{HOMO} = −IP = −5.68 eV) and LUMO at −2.4 eV, above that of **4e** (E_{LUMO} = −EA = −2.88 eV).

Fig. 7 presents the performance data of this device, which showed a turn on voltage of 5.1 V at 5 cd m^{-2} reaching a maximum luminance of 494 cd m^{-2} with a maximum EQE of 0.90% and a maximum current efficiency of 2.07 cd A^{-1}. The obtained EL spectrum (CIE coordinates at 100 cd m^{-2} of 0.28, 0.43) is slightly red shifted with respect to the PL spectra, which could be due to interference effects.

The OLEDs prepared with molecules **4e–4h** did not clearly show the phosphorescence contribution to the electroluminescence spectrum. In the case of **4g**, there is some indication that it may be present, but a definite conclusion cannot be drawn (see Fig. S18 in the ESI†). The absence of a clear phosphorescence contribution to the OLED emission is attributed to a significant charge-induced triplet quenching, promoted by the long lifetime of the triplets, which makes the observation of this emission very difficult.[16]

3. Conclusions

A set of halogen-substituted 2-iminopyrrolyl–BPh_2 complexes was synthesized and characterized in terms of their molecular and photophysical properties. The internal heavy-atom effect was strongly controlled by the position of the halogen atom in the *N*-aryl ring of the ligand moiety, being negligible for *para*-I substitution ($k_{isc} \approx 0.03$ ns^{-1}) and most effective for *ortho*-I substitution ($k_{isc} \approx 0.39$ ns^{-1}). Accordingly, complex **4h** exhibited the greatest phosphorescence emission at 77 K. DFT and TDDFT calculations reproduced well the absorption and emission energies and provided geometries of the first singlet and triplet excited states, which showed how the steric hindrance of the 2-substituents prevented the iminopyrrolyl ligands from achieving planarity in both situations. Evidence of spin–orbit coupling in the absorption spectra was only found for the molecules containing iodine and was more visible for the *ortho*-I derivative. OLEDs were fabricated based on solution processed and vacuum thermal evaporated films of complexes **4b–4h**, the best one giving an external quantum efficiency

(EQE_{max}) of 0.15% along with a luminance maximum (L_{max}) of 1812 cd m^{-2} for **4c**. An optimized structure was later prepared with 2-iminopyrrolyl boron complex **4e** as an emissive layer mixed with mCP as the host material. The latter structure gave rise to an improved EQE of nearly 1%, along with a maximum luminance of 494 cd m^{-2}.

4. Experimental section

4.1 General

All experiments dealing with air- and/or moisture-sensitive materials were carried out under inert atmosphere using a dual vacuum/nitrogen line and standard Schlenk techniques. Nitrogen gas was supplied by Air Liquide and purified by passage through 4 Å molecular sieves. Unless otherwise stated, all reagents were purchased from commercial suppliers (*e.g.* Acrös, Aldrich, Fluka, Alfa Aesar) and used without further purification. All solvents to be used under inert atmosphere were thoroughly deoxygenated and dehydrated before use. They were dried and purified by refluxing over a suitable drying agent followed by distillation under nitrogen. The following drying agents were used: sodium (for toluene and diethyl ether), calcium hydride (for *n*-hexane and dichloromethane). Solvents and solutions were transferred using a positive pressure of nitrogen through stainless steel cannulae and mixtures were filtered in a similar way using modified cannulae that could be fitted with glass fibre filter disks.

Nuclear magnetic resonance (NMR) spectra were recorded on a Bruker Avance III 300 spectrometer at 299.995 MHz (^{1}H), 75.4296 MHz (^{13}C) and 96.2712 MHz (^{11}B). Deuterated solvents were dried by storage over 4 Å molecular sieves and degassed by the freeze–pump–thaw method. Spectra were referenced internally using the residual protio solvent resonance (^{1}H) and the solvent carbon (^{13}C) resonances relative to tetramethylsilane (δ = 0) and referenced externally using 15% $BF_3.OEt_2$ (δ = 0) for ^{11}B. All chemical shifts are quoted in δ (ppm) and coupling constants given in hertz. Multiplicities were abbreviated as follows: broad (br), singlet (s), doublet (d), doublet of doublets (dd), triplet (t) and multiplet (m). For air- and/or moisture sensitive materials, samples were prepared in J. Young NMR tubes in a glove box. Elemental analyses were obtained from the IST elemental analysis services.

The reagent 2-formylpyrrole (**1**) was prepared according to the literature.[11] Materials used for the device fabrication were purchased from Sigma Aldrich (LiF(99.995%), TPD, TAPC), Alfa Aesar (Al wire (99.9995%)), and LUMTEC (TPBi, mCP, HAT-CN).

4.2 Syntheses

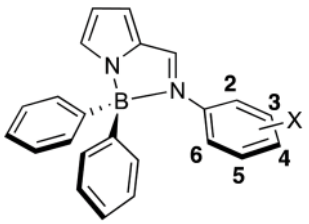

Synthesis of 2-(4-chlorophenylformimino)pyrrole (3c). 4-Chloroaniline **2c** (0.38 g, 3.0 mmol), 2-formylpyrrole **1** (0.28 g, 3.0 mmol) and a catalytic amount of *p*-toluenesulphonic acid were suspended in a mixture of xylenes (35 mL) in a 50 mL round-bottom flask fitted with a Soxhlet, a condenser and a $CaCl_2$ guard tube. The orange mixture was refluxed at ≈130 °C, for 4 days. After reaching room temperature, the reaction mixture was filtered, and all volatiles removed. The brown oil obtained was extracted with hot *n*-hexane, giving rise to an orange solution that was concentrated and kept at −20 °C. After some hours, a brown solid corresponding to the desired product **3c** was filtered and dried under vacuum. Yield, 0.15 g (25%). ^{1}H NMR (300 MHz, CD_2Cl_2): δ 9.47 (br, 1H, N*H*), 8.23 (s, 1H, C*H*═N), 7.33 (d, $^3J_{HH}$ = 9 Hz, 2H, N–Ph–H_3 + N–Ph–H_5), 7.11 (d, $^3J_{HH}$ = 9 Hz, 2H, N–Ph–H_2 + N–Ph–H_6), 6.98 (s, 1H, H5-*pyrr*), 6.70 (d, $^3J_{HH}$ = 3 Hz, 1H, H_3-*pyrr*), 6.32 (t, $^3J_{HH}$ = 3 Hz, 1H, H_4-*pyrr*).

Synthesis of 2-(4-bromophenylformimino)pyrrole (3d). 4-Bromoaniline **2d** (0.51 g, 3.0 mmol), 2-formylpyrrole **1** (0.28 g, 3.0 mmol), a catalytic amount of *p*-toluenesulphonic acid and $MgSO_4$ (to remove any water from the reaction mixture) were suspended in toluene (30 mL) in a 50 mL round-bottom flask fitted with a condenser and a $CaCl_2$ guard tube. The brown mixture was refluxed overnight, at 100 °C. After reaching room temperature, the reaction mixture was filtered, and all volatiles removed. The brown solid obtained was extracted with hot *n*-hexane, giving rise to a yellow solution that was concentrated and kept at −20 °C. After some hours, a beige solid corresponding to the desired product **3d** was filtered and dried under vacuum. Yield, 0.47 g (63%). ^{1}H NMR (300 MHz, CD_2Cl_2): δ 9.99 (br, 1H, N*H*), 8.24 (s, 1H, C*H*═N), 7.49 (d, $^3J_{HH}$ = 9 Hz, 2H, N–Ph–H_3 + N–Ph–H_5), 7.06 (d, $^3J_{HH}$ = 9 Hz, 2H, N–Ph–H_2 + N–Ph–H_6), 6.87 (s, 1H, H5-*pyrr*), 6.71 (d, $^3J_{HH}$ = 3 Hz, 1H, H_3-*pyrr*), 6.30 (t, $^3J_{HH}$ = 3 Hz, 1H, H_4-*pyrr*).

Synthesis of 2-(4-iodophenylformimino)pyrrole (3e). 4-Iodoaniline **2e** (0.66 g, 3.0 mmol), 2-formylpyrrole **1** (0.28 g, 3.0 mmol), a catalytic amount of *p*-toluenesulphonic acid and $MgSO_4$ (to remove any water from the reaction mixture) were suspended in toluene (30 mL) in a 50 mL round-bottom flask fitted with a condenser and a $CaCl_2$ guard tube. The brown mixture was refluxed at 100 °C, overnight. After reaching room temperature, the reaction mixture was filtered, all volatiles removed, and a small quantity of toluene added. The resulting brown solution was stored at −20 °C, giving a brown solid corresponding to the desired product **3e**. Yield, 0.36 g (41%). ^{1}H NMR (300 MHz, CD_2Cl_2): δ 9.81 (br, 1H, N*H*), 8.22 (s, 1H, C*H*═N), 7.68 (d, $^3J_{HH}$ = 9 Hz, 2H, N–Ph–H_3 + N–Ph–H_5), 6.96 (s, 2H, N–Ph–H_2 + N–Ph–H_6), 6.93 (s, 1H, H5-*pyrr*), 6.73 (d, $^3J_{HH}$ = 3 Hz, 1H, H_3-*pyrr*), 6.32 (t, $^3J_{HH}$ = 3 Hz, 1H, H_4-*pyrr*).

Synthesis of 2-(3-bromophenylformimino)pyrrole (3f). 3-Bromoaniline **2f** (1.72 g, 10.0 mmol), 2-formylpyrrole **1** (0.96 g, 10.1 mmol) and a catalytic amount of *p*-toluenesulphonic acid were suspended in toluene (30 mL) in a 50 mL round-bottom flask fitted with a Soxhlet apparatus, a condenser and a $CaCl_2$ guard tube. The orange mixture was refluxed at 130 °C, for 3 days. After reaching room temperature, the reaction mixture

was filtered, and all volatiles removed. The brown oil obtained was extracted with hot *n*-hexane, giving rise to a red solution that was concentrated and kept at −20 °C. After some hours, a brown solid corresponding to the desired product **3f** was filtered and dried under vacuum. Yield, 1.80 g (72%). ^{1}H NMR (300 MHz, CD_2Cl_2): δ 10.11 (br, 1H, N*H*), 8.26 (s, 1H, C*H*═N), 7.37 (s, 1H, N–Ph–H_2), 7.35 (s, 1H, N–Ph–H_4), 7.26 (t, $^3J_{HH}$ = 9 Hz, 1H, N–Ph–H_5), 7.15 (d, $^3J_{HH}$ = 3 Hz, 1H, N–Ph–H_6), 6.89 (s, 1H, H_5-*pyrr*), 6.76 (d, $^3J_{HH}$ = 3 Hz, 1H, H_3-*pyrr*), 6.33 (t, $^3J_{HH}$ = 3 Hz, 1H, H_4-*pyrr*). ^{13}C{^{1}H} NMR (75 MHz, $CDCl_3$): δ 153.3 (N–Ph–C_{ipso}), 150.9 (*C*H═N), 130.6 (N–Ph–C_5), 130.5 (C_2-*pyrr*), 128.4 (N–Ph–C_4), 124.1 (N–Ph–C_2), 123.9 (N–Ph–C_6), 122.9 (N–Ph–C_3), 120.2 (C_5-*pyrr*), 117.9 (C_3-*pyrr*), 110.8 (C_4-*pyrr*). Anal. calcd (%) for $C_{11}H_9BrN_2$: C, 53.04; H, 3.64; N, 11.25. Found: C, 53.06; H, 3.55; N, 11.14.

Synthesis of 2-(2-bromophenylformimino)pyrrole (3g). 2-Bromoaniline **2g** (1.73 g, 10.0 mmol), 2-formylpyrrole **1** (0.95 g, 10.0 mmol) and a catalytic amount of *p*-toluenesulphonic acid were suspended in toluene (30 mL) in a 50 mL round-bottom flask fitted with a Soxhlet apparatus, a condenser and a $CaCl_2$ guard tube. The orange mixture was refluxed at 130 °C, for 2 days. After reaching room temperature, the reaction mixture was filtered, and all volatiles removed. The brown oil obtained was extracted with hot *n*-hexane, giving rise to an orange solution that was concentrated and kept at −20 °C. After some hours, a beige solid corresponding to the desired product **3g** was filtered and dried under vacuum. Yield, 1.36 g (54%). ^{1}H NMR (300 MHz, CD_2Cl_2): δ 9.77 (br, 1H, N*H*), 8.11 (s, 1H, C*H*═N), 7.60 (d, $^3J_{HH}$ = 6 Hz, 1H, N–Ph–H_3), 7.29 (t, $^3J_{HH}$ = 6 Hz, 1H, N–Ph–H_5), 7–08–6.88 (m, 3H, N–Ph–H_4 + N–Ph–H_6 + H_5-*pyrr*), 6.70 (d, $^3J_{HH}$ = 3 Hz, 1H, H_3-*pyrr*), 6.30 (t, $^3J_{HH}$ = 3 Hz, 1H, H_4-*pyrr*). ^{13}C{^{1}H} NMR (75 MHz, $CDCl_3$): δ 150.9 (N–Ph–C_{ipso}), 150.6 (*C*H═N), 133.1 (N–Ph–C_3), 130.7 (C_2-*pyrr*), 128.6 (N–Ph–C_5), 126.4 (N–Ph–C_4), 123.7 (N–Ph–C_6), 120.1 (C_5-*pyrr*), 118.7 (N–Ph–C_2), 117.4 (C_3-*pyrr*), 110.8 (C_4-*pyrr*). Anal. calcd (%) for $C_{11}H_9BrN_2$: C, 53.04; H, 3.64; N, 11.25. Found: C, 53.07; H, 3.57; N, 11.25.

Synthesis of 2-(2-iodophenylformimino)pyrrole (3h). 2-Iodoaniline **2h** (0.50 g, 2.3 mmol), 2-formylpyrrole **1** (0.24 g, 2.5 mmol) and a catalytic amount of *p*-toluenesulphonic acid (*p*-TSA) were suspended in toluene (30 mL) in a 50 mL round-bottom flask fitted with a Soxhlet apparatus, a condenser and a $CaCl_2$ guard tube. The salmon-coloured mixture was refluxed overnight, at 130 °C. After reaching room temperature, the reaction mixture was filtered, and all volatiles were removed. The brown oil obtained was extracted with hot *n*-hexane, giving rise to a yellow solution that was concentrated and kept at −20 °C. After some hours, a brown solid corresponding to the desired product **3h** was filtered and dried under vacuum. Yield, 0.48 g (72%). ^{1}H NMR (300 MHz, CD_2Cl_2): δ 9.56 (br, 1H, N*H*), 8.10 (s, 1H, C*H*═N), 7.88 (d, $^3J_{HH}$ = 6 Hz, 1H, N–Ph–H_3), 7.35 (t, $^3J_{HH}$ = 6 Hz, 1H, N–Ph–H_5), 7.06–6.94 (m, 2H, N–Ph–H_6 + H_5-*pyrr*), 6.89 (t, $^3J_{HH}$ = 6 Hz, 1H, N–Ph–H_4), 6.72 (s, 1H, H_3-*pyrr*), 6.33 (s, 1H, H_4-*pyrr*). ^{13}C{^{1}H} NMR (75 MHz, $CDCl_3$): δ 152.7 (N–Ph–C_{ipso}), 150.0 (*C*H═N), 139.2 (N–Ph–C_3), 130.5 (C_2-*pyrr*), 129.5 (N–Ph–C_5), 126.7 (N–Ph–C_4), 123.4 (N–Ph–C_6), 118.5 (C_5-*pyrr*), 116.9 (C_3-*pyrr*), 110.9 (C_4-*pyrr*), 95.6 (N–Ph–C_2). Anal. calcd (%) for $C_{11}H_9IN_2$: C, 44.62; H, 3.06; N, 9.46. Found: C, 44.70; H, 3.07; N, 9.41.

Synthesis of [BPh$_2${κ^2*N*,*N*′-NC$_4$H$_3$C(H)═N-4-Cl-C$_6$H$_4$}] (4c). A solution of 2-(4-chlorophenylformimino)pyrrole **3c** (0.20 g, 1.0 mmol), in toluene, was added to triphenylboron (0.24 g, 1.0 mmol) (also in toluene). The green solution was refluxed under nitrogen overnight. The resulting dark green solution was cooled to room temperature, filtered and all volatiles removed under vacuum. Crystals of the desired boron complex **4c** suitable for single crystal X-ray diffraction studies were obtained by double layering with toluene and *n*-hexane. The solution was filtered, and the crystals dried under vacuum. Yield, 0.17 g (47%). ^{1}H NMR (300 MHz, CD_2Cl_2): δ 8.48 (s, 1H, C*H*═N), 7.31–7.16 (m, 15H, N–Ph–H_2 + N–Ph–H_3 + N–Ph–H_5 + N–Ph–H_6 + B–Ph–H_{ortho} + B–Ph–H_{meta} + B–Ph–H_{para} + H_5-*pyrr*), 7.08 (d, $^3J_{HH}$ = 3 Hz, 1H, H_3-*pyrr*), 6.58 (dd, $^3J_{HH}$ = 6 Hz, $^4J_{HH}$ = 3 Hz, 1H, H_4-*pyrr*). ^{13}C{^{1}H} NMR (75 MHz, $CDCl_3$): δ 150.8 (*C*H═N), 141.2 (N–Ph–C_{ipso}), 134.7 (C_2-*pyrr*), 133.5 (B–Ph–C_{ortho}), 133.1 (N–Ph–C_4), 132.3 (C_5-*pyrr*), 129.8 (N–Ph–C_3 + N–Ph–C_5), 127.9 (B–Ph–C_{meta}), 127.1 (B–Ph–C_{para}), 123.8 (N–Ph–C_2 + N–Ph–C_6), 118.0 (C_4-*pyrr*), 116.0 (C_3-*pyrr*), B–Ph–C_{ipso} resonance absent. ^{11}B NMR (96.29 MHz, CD_2Cl_2): δ 4.73. Anal. calcd (%) for $C_{23}H_{18}BClN_2$: C, 74.93; H, 4.92; N, 7.60. Found: C, 75.09; H, 4.94; N, 7.67.

Synthesis of [BPh$_2${κ^2*N*,*N*′-NC$_4$H$_3$C(H)═N-4-Br-C$_6$H$_4$}] (4d). A solution of 2-(4-bromophenylformimino)pyrrole **3d** (0.45 g, 1.8 mmol), in toluene, was added to triphenylboron (0.44 g, 1.8 mmol) (also in toluene). The yellow solution was refluxed under nitrogen overnight. The resulting dark green solution was cooled to room temperature, and the solvent concentrated under vacuum and stored at −20 °C. In the following day, crystals of the desired boron complex **4d** suitable for single crystal X-ray diffraction studies were obtained. The solution was filtered, and the crystals dried under vacuum. Yield, 0.34 g (45%). ^{1}H NMR (300 MHz, CD_2Cl_2): δ 8.49 (s, 1H, C*H*═N), 7.41 (d, $^3J_{HH}$ = 9 Hz, 2H, N–Ph–H_3 + N–Ph–H_5), 7.31–7.18 (m, 11H, H_5-*pyrr* + B–Ph–C_{ortho} + B–Ph–C_{meta} + B–Ph–C_{para}), 7.15 (d, $^3J_{HH}$ = 9 Hz, 2H, N–Ph–H_2 + N–Ph–H_6), 7.09 (dd, $^3J_{HH}$ = 6 Hz, $^4J_{HH}$ = 3 Hz, 1H, H_3-*pyrr*), 6.58 (dd, $^3J_{HH}$ = 6 Hz, $^4J_{HH}$ = 3 Hz, 1H, H_4-*pyrr*). ^{13}C{^{1}H} NMR (75 MHz, $CDCl_3$): δ 150.7 (*C*H═N), 141.6 (N–Ph–C_{ipso}), 134.8 (C_2-*pyrr*), 133.5 (B–Ph–C_{ortho}), 132.8 (N–Ph–C_3 + N–Ph–C_5), 132.3 (C_5-*pyrr*), 128.0 (B–Ph–C_{meta}), 127.1 (B–Ph–C_{para}), 124.0 (N–Ph–C_2 + N–Ph–C_6), 121.0 (N–Ph–C_4), 118.1 (C_4-*pyrr*), 116.1 (C_3-*pyrr*), B–Ph–C_{ipso} resonance absent. ^{11}B NMR (96.29 MHz, CD_2Cl_2): δ 4.77. Anal. calcd (%) for $C_{23}H_{18}BBrN_2$: C, 66.87; H, 4.39; N, 6.78. Found: C, 66.72; H, 4.36; N, 6.83.

Synthesis of [BPh$_2${κ^2*N*,*N*′-NC$_4$H$_3$C(H)═N-4-I-C$_6$H$_4$}] (4e). A solution of 2-(4-iodophenylformimino)pyrrole **3e** (0.36 g, 1.2 mmol), in toluene, was added to triphenylboron (0.29 g, 1.2 mmol) (also in toluene). The greenish yellow solution was refluxed overnight under nitrogen. The resulting solution was cooled to room temperature and all volatiles removed under vacuum. A green powder of the desired boron complex **4e** was obtained by double layering a toluene solution with *n*-hexane.

The solution was filtered, and the powder dried under vacuum. Yield, 0.25 g (45%). ^{1}H NMR (300 MHz, CD_2Cl_2): δ 8.50 (s, 1H, C*H*=N), 7.60 (d, $^3J_{HH}$ = 9 Hz, 2H, N–Ph–H_3 + N–Ph–H_5), 7.33–7.14 (m, 11H, H_5-*pyrr* + B–Ph–H_{ortho} + B–Ph–H_{meta} + B–Ph–H_{para}), 7.08 (d, $^3J_{HH}$ = 6 Hz, 1H, H_3-*pyrr*), 7.03 (d, $^3J_{HH}$ = 9 Hz, 2H, N–Ph–H_2 + N–Ph–H_6), 6.58 (dd, $^3J_{HH}$ = 6 Hz, $^4J_{HH}$ = 3 Hz, 1H, H_4-*pyrr*). ^{13}C{^{1}H} NMR (75 MHz, $CDCl_3$): δ 150.5 (*C*H=N), 142.2 (N–Ph–C_{ipso}), 138.8 (N–Ph–C_3 + N–Ph–C_5), 134.8 (C_2-*pyrr*), 133.5 (B–Ph–C_{ortho}), 132.4 (C_5-*pyrr*), 128.0 (B–Ph–C_{meta}), 127.1 (B–Ph–C_{para}), 124.2 (N–Ph–C_2 + N–Ph–H_6), 118.1 (C_4-*pyrr*), 116.1 (C_3-*pyrr*), 92.2 (N–Ph–C_4), B–Ph–C_{ipso} resonance absent. ^{11}B NMR (96.29 MHz, CD_2Cl_2): δ 5.05. Anal. calcd (%) for $C_{23}H_{18}BIN_2$: C, 60.04; H, 3.94; N, 6.09. Found: C, 60.07; H, 3.93; N, 6.08.

Synthesis of [BPh$_2${κ^2*N*,*N*′-NC$_4$H$_3$C(H)=N-3-Br-C$_6$H$_4$}] (4f). A solution of 2-(3-bromophenylformimino)pyrrole **3f** (0.57 g, 2.3 mmol), in toluene, was added to triphenylboron (0.55 g, 2.3 mmol) (also in toluene). The green solution was refluxed overnight under nitrogen. The resulting dark green solution was cooled to room temperature and filtered. The solvent was concentrated under vacuum and the final solution stored at −20 °C, giving rise to a yellow powder corresponding to the desired boron complex **4f**, which was dried under vacuum. Yield, 0.25 g (45%). ^{1}H NMR (300 MHz, CD_2Cl_2): δ 8.48 (s, 1H, C*H*=N), 7.40 (s, 1H, N–Ph–H_2), 7.37 (d, $^3J_{HH}$ = 9 Hz, 1H, N–Ph–H_4), 7.33–7.18 (m, 12H, N–Ph–H_6 + B–Ph–H_{ortho} + B–Ph–H_{meta} + B–Ph–H_{para} + H_5-*pyrr*), 7.16 (d, $^3J_{HH}$ = 9 Hz, 1H, N–Ph–H_5), 7.10 (d, $^3J_{HH}$ = 3 Hz, 1H, H_3-*pyrr*), 6.59 (dd, $^3J_{HH}$ = 6 Hz, $^4J_{HH}$ = 3 Hz, 1H, H_4-*pyrr*). ^{13}C{^{1}H} NMR (75 MHz, $CDCl_3$): δ 150.9 (*C*H=N), 143.8 (N–Ph–C_{ipso}), 134.7 (C_2-*pyrr*), 133.5 (B–Ph–C_{ortho}), 132.6 (C_5-*pyrr*), 130.9 (N–Ph–C_5), 130.5 (N–Ph–C_4), 128.0 (B–Ph–C_{meta}), 127.2 (B–Ph–C_{para}), 125.2 (N–Ph–C_2), 123.1 (N–Ph–C_3), 121.4 (N–Ph–C_6), 118.3 (C_4-*pyrr*), 116.4 (C_3-*pyrr*), B–Ph–C_{ipso} resonance absent. ^{11}B NMR (96.29 MHz, CD_2Cl_2): δ 5.09. Anal. calcd (%) for $C_{23}H_{18}BBrN_2$: C, 66.87; H, 4.39; N, 6.78. Found: C, 66.81; H, 4.23; N, 6.73.

Synthesis of [BPh$_2${κ^2*N*,*N*′-NC$_4$H$_3$C(H)=N-2-Br-C$_6$H$_4$}] (4g). A solution of 2-(2-bromophenylformimino)pyrrole **3g** (0.46 g, 1.8 mmol), in toluene, was added to triphenylboron (0.47 g, 1.9 mmol) (also in toluene). The greenish blue solution was refluxed under nitrogen overnight. The resulting dark blue solution was cooled to room temperature, the solvent concentrated under vacuum and stored at −20 °C. In the following day, crystals of the desired boron complex **4g** suitable for single crystal X-ray diffraction studies were obtained. The solution was filtered, and the crystals dried under vacuum. Yield, 0.39 g (53%). ^{1}H NMR (300 MHz, CD_2Cl_2): δ 8.31 (s, 1H, C*H*=N), 7.58 (dd, $^3J_{HH}$ = 6 Hz, $^4J_{HH}$ = 3 Hz, 1H, N–Ph–H_3), 7.29 (s, 1H, N–Ph–H_5), 7.25–7.03 (m, 13H, N–Ph–H_4 + H_3-*pyrr* + H_5-*pyrr* + B–Ph–H_{ortho} + B–Ph–H_{meta} + B–Ph–H_{para}), 6.95 (dd, $^3J_{HH}$ = 6 Hz, $^4J_{HH}$ = 3 Hz, 1H, N–Ph–H_6), 6.66 (dd, $^3J_{HH}$ = 6 Hz, $^4J_{HH}$ = 3 Hz, 1H, N–Ph–H_4). ^{13}C{^{1}H} NMR (75 MHz, $CDCl_3$): δ 156.4 (*C*H=N), 141.5 (N–Ph–C_{ipso}), 135.1 (C_2-*pyrr*), 134.1 (N–Ph–C_3), 133.4 (B–Ph–C_{ortho}), 132.4 (N–Ph–C_5), 129.4 (C_5-*pyrr*), 128.2 (N–Ph–C_4), 127.8 (B–Ph–C_{meta}), 127.4 (N–Ph–C_6), 126.9 (B–Ph–C_{para}), 119.9 (N–Ph–C_2), 117.6 (C_4-*pyrr*), 116.0 (C_3-*pyrr*), B–Ph–C_{ipso} resonance absent. ^{11}B NMR (96.29 MHz, CD_2Cl_2): δ 5.34. Anal. calcd (%) for $C_{23}H_{18}BBrN_2$: C, 66.87; H, 4.39; N, 6.78. Found: C, 66.96; H, 4.26; N, 6.76.

Synthesis of [BPh$_2${κ^2*N*,*N*′-NC$_4$H$_3$C(H)=N-2-I-C$_6$H$_4$}] (4h). A solution of 2-(2-iodophenylformimino)pyrrole **3h** (0.31 g, 1.0 mmol), in toluene, was added to triphenylboron (0.25 g, 1.0 mmol) (also in toluene). The orange solution was refluxed overnight under nitrogen. The resulting dark brown suspension was cooled to room temperature and all volatiles removed under vacuum. The brown powder of the desired boron complex **4h** was obtained by double layering a toluene solution with *n*-hexane. The solution was filtered, and the powder dried under vacuum. Yield, 0.33 g (69%). ^{1}H NMR (300 MHz, CD_2Cl_2): δ 8.26 (s, 1H, C*H*=N), 7.83 (d, $^3J_{HH}$ = 9 Hz, 1H, N–Ph–H_3), 7.29 (t, $^3J_{HH}$ = 9 Hz, 1H, N–Ph–H_4), 7.26–7.04 (m, 12H, H_3-*pyrr* + H_5-*pyrr* + B–Ph–H_{ortho} + B–Ph–H_{meta} + B–Ph–H_{para}), 7.00 (t, $^3J_{HH}$ = 9 Hz, 1H, N–Ph–H_4), 6.90 (d, $^3J_{HH}$ = 9 Hz, 1H, N–Ph–H_6), 6.67 (s, 1H, H_4-*pyrr*). ^{13}C{^{1}H} NMR (75 MHz, $CDCl_3$): δ 156.3 (*C*H=N), 144.7 (N–Ph–C_{ipso}), 140.6 (N–Ph–C_3), 134.2 (C_2-*pyrr*), 133.5 (B–Ph–C_{ortho}), 132.4 (N–Ph–C_5), 129.6 (N–Ph–C_4), 129.0 (C_5-*pyrr*), 127.7 (B–Ph–C_{meta}), 126.9 (B–Ph–C_{para}), 126.7 (N–Ph–C_6), 117.5 (C_4-*pyrr*), 115.8 (C_3-*pyrr*), 96.1 (N–Ph–C_2), B–Ph–C_{ipso} resonance absent. ^{11}B NMR (96.29 MHz, CD_2Cl_2): δ 5.31. Anal. calcd (%) for $C_{23}H_{18}BIN_2$: C, 60.04; H, 3.94; N, 6.09. Found: C, 60.36; H, 3.94; N, 6.04.

4.3 X-ray data collection

The crystallographic data for complexes **4c**, **4d** and **4g** were collected using graphite monochromated Mo-Kα radiation (λ = 0.71073 Å) on a Bruker AXS-KAPPA APEX II diffractometer equipped with an Oxford Cryosystem open-flow nitrogen cryostat, at 150 K, and the crystals were selected under inert atmosphere, stored in polyfluoroether oil and mounted on a nylon loop. Cell parameters were retrieved using Bruker SMART software and refined using Bruker SAINT on all observed reflections. Absorption corrections were applied using SADABS.[17] Structure solution and refinement were performed using direct methods with the programs SIR2004,[18] SIR2014,[19] SIR2018 (ref. 19) and SHELXL,[20] included in the package of programs WINGX-Version2014.1.[21] All hydrogen atoms were inserted in idealized positions and allowed to refine riding on the parent carbon atom, with C–H distances of 0.95 Å for aromatic H atoms and with U_{iso}(H) = 1.2U_{eq}(C). Graphic presentations were prepared with ORTEP-III.[21] Data were deposited in CCDC under the deposit numbers 2004594 for **4c**, 2004595 for **4d**, and 2004596 for **4g**.†

4.4 Cyclic voltammetry measurements

Cyclic voltammetry (CV) measurements were performed on a Solartron potentiostat in a three-electrode cell with a 0.1 M tetrabutylammonium perchlorate (TBAClO$_4$)/CH_2Cl_2 supporting electrolyte, at a scan rate of 50 mV s^{-1}, at room temperature and under inert atmosphere (N_2). The reference electrode, counter electrode and working electrode used were a saturated calomel electrode (SCE), a platinum wire and a platinum disk, respectively.

4.5 Spectroscopic measurements

An Agilent Cary 8454 UV-Visible spectrophotometer and a SPEX Fluorolog 212I were used to obtain the absorption and fluorescence spectra of **4c–4h** solutions, in THF. The fluorescence spectra were collected with right angle geometry, in the S/R mode, and corrected for instrumental wavelength dependence. Fluorescence quantum yields were determined by comparison with the quantum yields of α-tetrathiophene (for complexes **4c–4f**) and α-terthiophene (for complexes **4g** and **4h**) in dioxane at 25 °C. Phosphorescence spectra were measured with a SPEX 1934D phosphorimeter using a time window of 20 ms.

Fluorescence decays were measured using the time-correlated single photon counting technique with a previously described home-made apparatus.[22] Briefly, the excitation pulses were provided by the frequency-doubled emission of a Millennia Xs/Tsunami lasers system from Spectra Physics, operating at 82 MHz and detected with a microchannel plate photomultiplier (Hamamatsu R3809u-50). The FWHM of the instrumental response function (IRF) (obtained with an optically matched scattering Ludox solution) is *ca.* 18 ps with 814 fs/channel resolution. Fluorescence decays were deconvoluted from the excitation pulse using the modulation functions method (Sand program).[23]

For solid state measurements, toluene solutions of each complex **4c–4h** (at a concentration of 1 mg mL^{-1}) and ZEONEX® 480 (at a concentration of 100 mg mL^{-1}) were blended on a ratio of 1 wt% and drop-cast (~80 μL) at 30 °C. ZEONEX® 480 is a transparent ethylene-cycloolefin copolymer.[24]

Absorption and emission spectra of the ZEONEX samples were collected using a UV-3600 double beam spectrophotometer (Shimadzu) and Jobin Yvon Horiba FluoroMax 3. Lifetime measurements were obtained by exciting the solid state samples with a pulsed Nd:YAG laser (EKSPLA), at 355 nm.[25] Photoluminescence quantum yield measurements[26] were performed using an integration sphere coupled with a sensitive QePro spectrometer (Ocean Optics) using a 365 nm LED light source (Ocean Optics). The photoluminescence lifetimes were obtained using time correlated single photon counting (Mira-900 picosecond laser system).

The experimental setup used to obtain triplet absorption spectra and triplet lifetimes consists of an Applied Photophysics laser flash photolysis apparatus pumped by the third harmonic (355 nm) of a Nd:YAG laser (Spectra Physics). The detection system (Hamamatsu R928 photomultipliers) is at right angles to the excitation beam, and a pulsed 150 W Xe lamp was used to analyse the transient absorption. The signal obtained was fed into a Tektronix TDS 3052B digital analyser and transferred to an IBM RISC computer where the optical density (OD) at different wavelengths and different delays after flash were collected using the appropriate software (Applied photophysics). Transient absorption spectra were collected by monitoring the optical density change at intervals of 10 nm over the range of 330–650 nm and averaging at least 10 decays at each wavelength. First order kinetics was observed for the decays of the lowest triplet state, except for complex **4h**. Special care was taken in order to have sufficiently low laser energies (≤2 mJ) to avoid multiphoton and/or triplet–triplet annihilation effects. Before the experiments were done, all solutions were degassed with nitrogen for ≈20 min and sealed. The triplet molar absorption coefficients obtained in THF were determined by the singlet depletion technique, according to the well-known relationship, $\varepsilon_T = \varepsilon_S \times \Delta OD_T/\Delta OD_S$.[27] The Φ_T values were measured using benzophenone in toluene as the reference compound, $\Phi_T^{cp} = \Phi_T^{ref} \times (\varepsilon_T^{ref} \times \Delta OD_T^{cp})/(\varepsilon_T^{cp} \times \Delta OD_T^{ref})$.

4.6 Computational studies

The ADF program (Amsterdam Density Functional)[28–30] was used in all Density Functional Theory calculations.[31] The geometries of **4a–h** were optimized without symmetry constraints, with the Vosko–Wilk–Nusair[32] Local Density Approximation of the correlation energy and the PBE0 functional,[33,34] with spin orbit coupling (SOPERT),[35] taking into account solvent effects (THF) with the COSMO model implemented in ADF. Relativistic effects were treated with the ZORA approximation.[36] Triple ζ Slater-type orbitals (STO) were used to describe all the electrons of H, C, B, N, F, Cl, Br, and I, augmented with a set of one polarization function (H, single ζ 2s; C, B, N, F, Cl single ζ, 3d; Br single ζ, 4d; I single ζ, 5d). TDDFT was used to obtain the geometry of the first singlet excited states[37–40] and to obtain the absorption spectra with the Tamm–Dancoff approximation (TDA).[41] Unrestricted calculations were carried out for open shell complexes. The starting geometries were the experimental ones described above for **4c–d**, and **4g**, or modelled after them. The excited singlet state lifetimes were obtained from the SOPERT calculations and the calculated fluorescence rate constants were their reciprocal.

For the sake of comparison with previous studies and to evaluate the role of dispersion in these systems, the previous calculations (method A in the ESI†) were repeated with the B3LYP functional (method B),[42] with PBE0 and the Grimme D3 correction[43] (A/D3), with B3LYP and the Grimme D3 correction (B/D3), with Becke's exchange[44] and Perdew's[45,46] correlation functionals (gas phase, GP). The basis set was TZP with a small frozen core for all atoms. The solvent (COSMO) was introduced in a single point calculation on the structure from the latter. The same structure was used to calculate the absorption spectra with (THF) and without solvent (GP) and, also in gas phase and SOPERT, to obtain excited state lifetimes (SO). The first singlet excited state was obtained by the promotion of one electron from the HOMO to the LUMO followed by geometry optimization.

4.7 Light-emitting diode studies

The results presented in Table 5 and in the ESI† refer to OLEDs where the complexes were used in the neat form (deposited by either spin coating or vacuum thermal deposition) or dispersed in poly(vinylcarbazole). These devices were tested under vacuum, using a K2400 Source Meter and a calibrated silicon photodiode, as described before.[47] The electroluminescence (EL) spectra were obtained with a CCD spectrograph

(Ocean Optics or ScanSci). External quantum efficiency values were estimated as described previously.[47]

The ITO/HAT-CN/TAPC/mCP co 10% **4e**/TPBi/LiF/Al device was fabricated with pre-cleaned indium–tin–oxide (ITO) coated glass substrate after ozone plasma treatment. HAT-CN was used as a hole injection layer and TAPC as a hole transport layer. The emissive layer consisted of **4e** co-evaporated with mCP (1,3-bis-(*N*-carbazolyl)benzene) to give 10% contribution of emitter by keeping the evaporation rate in proportion of 1 : 9 for emitter and host, respectively. TPBi was used as the electron transport layer. All organic and inorganic layers were thermally deposited using the Kurt J. Lesker Spectros II deposition system at 10^{-6} mbar. The deposition rate was kept at 1 Å s^{-1} for all layers except for LiF and the emissive material in co-evaporation in which case they were kept at 0.1–0.2 Å s^{-1}. The device was characterized using a 10 inch integrating sphere (Labsphere) coupled with a USB spectrometer (Ocean Optics) and connected to a Source Measure Unit.

Conflicts of interest

There are no conflicts to declare.

Acknowledgements

We thank the Fundação para a Ciência e a Tecnologia for financial support (Project PTDC/QUI-QIN/31585/2017) and for fellowships to A.I.R., P. K., C. S. B. G. and M. J. C. (PD/BD/113535/2015 – ChemMat PhD Program, SFRH/BPD/89167/2012, SFRH/BPD/107834/2015 and SFRH/BSAB/135473/2017, respectively). Centro de Química Estrutural, BioISI – Biosystems & Integrative Sciences Institute, Centro de Química de Coimbra, Instituto de Telecomunicações, Associate Laboratory for Green Chemistry – LAQV, and Applied Molecular Biosciences Unit – UCIBIO acknowledge the Fundação para a Ciência e Tecnologia for financial support (Projects UIDB/00100/2020 and UIDP/00100/2020, UIDB/04046/2020 and UIDP/04046/2020, UIDB/00313/2020 and UIDP/00313/2020, UIDB/50008/2020, UIDB/50006/2020, and UIDB/04378/2020, respectively). M. J. C. thanks Christophe Gourlaouen, University of Strasbourg, France, for helpful discussions.

References

1 C. W. Tang and S. A. Van Slyke, *Appl. Phys. Lett.*, 1987, **51**, 913.

2 (*a*) C. W. Lee, O. Y. Kim, J. Y. Lee and J. Ind, *Eng. Chem.*, 2014, **20**, 1198–1208; (*b*) N. T. Kalyani and S. J. Dhoble, *Renewable Sustainable Energy Rev.*, 2015, **44**, 319–347; (*c*) J.-H. Jou, S. Kumar, A. Agrawal, T.-H. Li and S. Sahoo, *J. Mater. Chem. C*, 2015, **3**, 2974; (*d*) H.-J. Li, W.-F. Fu, L. Li, X. Gan, W.-H. Mu, W.-Q. Chen, X.-M. Duan and H.-B. Song, *Org. Lett.*, 2010, **12**, 2924–2927; (*e*) C. Adachi, T. Tsutsui and S. Saito, *Appl. Phys. Lett.*, 1990, **56**, 799; (*f*) J. Ye, Z. Chen, M.-K. Fung, C. Zheng, X. Ou, X. Zhang, Y. Yuan and C.-S. Lee, *Chem. Mater.*, 2013, **25**, 2630–2637; (*g*) S. Kappaun, C. Slugovc and E. J. W. List, *Int. J. Mol. Sci.*, 2008, **9**, 1527–1547; (*h*) X.-C. Hang, T. Fleetham, E. Turner, J. Brooks and J. Li, *Angew. Chem., Int. Ed.*, 2013, **52**, 1–5; (*i*) A. Tronnier, A. Risler, N. Langer, G. Wagenblast, I. Münster and T. Strassner, *Organometallics*, 2012, **31**, 7447–7452; (*j*) M. A. Baldo, D. F. O'Brien, Y. You, A. Shoustikov, S. Sibley, M. E. Thompson and S. R. Forrest, *Nature*, 1998, **395**, 151–154; (*k*) Z. Zhong, X. Wang, Y. Ma, F. Peng, T. Guo, J.-X. Jiang, L. Ying, J. Wang, J. Peng and Y. Cao, *Org. Electron.*, 2018, **57**, 178–185; (*l*) Y.-X. Hu, X. Xia, W.-Z. He, Z.-J. Tang, Y.-L. Lv, X. Li and D.-Y. Zhang, *Org. Electron.*, 2019, **66**, 126–135; (*m*) G. Li, D. G. Congrave, D. Zhu, Z. Su and M. R. Bryce, *Polyhedron*, 2018, **140**, 146–157; (*n*) C. Bizzarri, F. Hundemer, J. Busch and S. Bräse, *Polyhedron*, 2018, **140**, 51–66; (*o*) P. Data, P. Pander, M. Okazaki, Y. Takeda, S. Minakata and A. P. Monkman, *Angew. Chem., Int. Ed.*, 2016, **55**, 5739–5744; (*p*) H. Wang, Y. Liu, W. Hu, W. Xu, P. Wang, Y. Wang and X. Luan, *Org. Electron.*, 2018, **61**, 376–382; (*q*) T. Hatakeyama, K. Shiren, K. Nakajima, S. Nomura, S. Nakatsuka, K. Kinoshita, J. Ni, Y. Ono and T. Ikuta, *Adv. Mater.*, 2016, **28**, 2777–2781; (*r*) Y. Wada, K. Shizu, S. Kubo, K. Suzuki, H. Tanaka and C. Adachi, *Appl. Phys. Lett.*, 2015, **107**, 105–110; (*s*) S. Wang, X. Yan, Z. Cheng, H. Zhang, Y. Liu and Y. Wang, *Angew. Chem., Int. Ed.*, 2015, **54**, 13068–13072; (*t*) H. Uoyama, K. Goushi, K. Shizu, H. Nomura and C. Adachi, *Nature*, 2012, **492**, 234–238; (*u*) Y.-J. Shiu, Y.-C. Cheng, W.-L. Tsai, C.-C. Wu, C.-T. Chao, C.-W. Lu, Y. Chi, Y.-T. Chen, S.-H. Liu and P.-T. Chou, *Angew. Chem., Int. Ed.*, 2016, **55**, 3017–3021; (*v*) B. M. Bell, T. P. Clark, T. S. De Vries, Y. Lai, D. S. Laitar, T. J. Gallagher, J.-H. Jeon, K. L. Kearns, T. McIntire, S. Mukhopadhyay, H.-Y. Na, T. D. Paine and A. A. Rachford, *Dyes Pigm.*, 2017, **141**, 83–92; (*w*) Y.-J. Shiu, Y.-T. Chen, W.-K. Lee, C.-C. Wu, T.-C. Lin, S.-H. Liu, P.-T. Chou, C.-W. Lu, I.-C. Cheng, Y.-J. Lien and Y. Chi, *J. Mater. Chem. C*, 2017, **5**, 1452–1462; (*x*) K. Matsuo and T. Yasuda, *Chem. Commun.*, 2017, **53**, 8723–8726; (*y*) M. Stanoppi and A. Lorbach, *Dalton Trans.*, 2018, **47**, 10394–10398.

3 (*a*) D. Li, H. Zhang and Y. Wang, *Chem. Soc. Rev.*, 2013, **42**, 8416–8433; (*b*) D. Frath, J. Massue, G. Ulrich and R. Ziessel, *Angew. Chem., Int. Ed.*, 2014, **53**, 2290–2310; (*c*) D. Suresh and P. T. Gomes, in *Advances in Organometallic Chemistry and Catalysis*, ed. A. J. L. Pombeiro, John Wiley & Sons, Inc., Hoboken, NJ, USA, 2014, ch. 36, pp. 485–492; (*d*) S.-F. Liu, Q. Wu, H. L. Schmider, H. Aziz, N.-X. Hu, Z. Popovic and S. Wang, *J. Am. Chem. Soc.*, 2000, **122**, 3671–3678; (*e*) S. Anderson, M. S. Weaver and A. J. Hudson, *Synth. Met.*, 2000, **111–112**, 459–463; (*f*) Y. Liu, J. Guo, H. Zhang and Y. Wang, *Angew. Chem., Int. Ed.*, 2002, **41**, 182–184; (*g*) H.-Y. Chen, Y. Chi, C.-S. Liu, J.-K. Yu, Y.-M. Cheng, K.-S. Chen, P.-T. Chou, S.-M. Peng, G.-H. Lee, A. J. Carty, S.-J. Yeh and C.-T. Chen, *Adv. Funct. Mater.*, 2005, **15**, 567–574; (*h*) Q. D. Liu, M. S. Mudadu, R. Thummel, Y. Tao and

S. Wang, *Adv. Funct. Mater.*, 2005, **15**, 143–154; (*i*) J. Ugolotti, S. Hellstrom, G. J. P. Britovsek, T. S. Jones, P. Hunt and A. J. P. White, *Dalton Trans.*, 2007, **14**, 1425–1432; (*j*) Z. Zhang, H. Bi, Y. Zhang, D. Yao, H. Gao, Y. Fan, H. Zhang, Y. Wang, Y. Wang, Z. Chen and D. Ma, *Inorg. Chem.*, 2009, **48**, 7230–7236; (*k*) D. Li, Z. Zhang, S. Zhao, Y. Wang and H. Zhang, *Dalton Trans.*, 2011, **40**, 1279–1285; (*l*) Y.-L. Rao and S. Wang, *Inorg. Chem.*, 2011, **50**, 12263–12274; (*m*) Y.-J. Shiu, Y.-C. Cheng, W.-L. Tsai, C.-C. Wu, C.-T. Chao, C.-W. Lu, Y. Chi, Y.-T. Chen, S.-H. Liu and P.-T. Chou, *Angew. Chem., Int. Ed.*, 2016, **55**, 3017–3021.

4 (*a*) B. Lee, B. G. Park, W. Cho, H. Y. Lee, A. Olasz, C.-H. Chen, S. B. Park and D. Lee, *Chem. – Eur. J.*, 2016, **22**, 17321–17328; (*b*) B. M. Bell, T. P. Clark, T. S. De Vries, Y. Lai, D. S. Laitar, T. J. Gallagher, J.-H. Jeon, K. L. Kearns, T. McIntire, S. Mukhopadhyay, H.-Y. Na, T. D. Paine and A. A. Rachford, *Dyes Pigm.*, 2017, **141**, 83–92; (*c*) K. Matsuo and T. Yasuda, *Chem. Commun.*, 2017, **53**, 8723–8726; (*d*) Y.-J. Shiu, Y.-T. Chen, W.-K. Lee, C.-C. Wu, T.-C. Lin, S.-H. Liu, P.-T. Chou, C.-W. Lu, I.-C. Cheng, Y.-J. Lien and Y. Chi, *J. Mater. Chem. C*, 2017, **5**, 1452–1462; (*e*) Y. Wu, W. Yuan, H. Ji, Y. Qin, J. Zhang, H. Li, Y. Li, Y. Wang, Y. Sun and W. Liu, *Dyes Pigm.*, 2017, **142**, 330–339; (*f*) H. Zhang, C. Liu, J. Xiu and J. Qiu, *Dyes Pigm.*, 2017, **136**, 798–806; (*g*) M. Stanoppi and A. Lorbach, *Dalton Trans.*, 2018, **47**, 10394–10398; (*h*) K. Dhanunjayarao, V. Mukundam, R. V. R. N. Chinta and K. Venkatasubbaiah, *J. Organomet. Chem.*, 2018, **865**, 234–238; (*i*) F. Yagishita, T. Kinouchi, K. Hoshi, Y. Tezuka, Y. Jibu, T. Karatsu, N. Uemura, Y. Yoshida, T. Mino, M. Sakamoto and Y. Kawamura, *Tetrahedron*, 2018, **74**, 3728–3733; (*j*) D. Wang, Y.-P. Wan, H. Liu, D.-J. Wang and G.-D. Yin, *Dyes Pigm.*, 2018, **149**, 728–735; (*k*) C. C. Vidyasagar, B. M. M. Flores, V. M. Jiménez-Pérez and P. M. Gurubasavaraj, *Mater. Today Chem.*, 2019, **11**, 133–155; (*l*) X. Li, P. Tang, T. Yu, W. Su, Y. Li, Y. Wang, Y. Zhao and H. Zhang, *Dyes Pigm.*, 2019, **163**, 9–16; (*m*) D. Song, Y. Yu, L. Yue, D. Zhong, Y. Zhang, X. Yang, Y. Sun, G. Zhou and Z. Wu, *J. Mater. Chem. C*, 2019, **7**, 11953–11963; (*n*) P. Li, H. Chan, S.-L. Lai, M. Ng, M.-Y. Chan and V. W.-W. Yam, *Angew. Chem., Int. Ed.*, 2019, **58**, 9088–9094.

5 (*a*) D. Suresh, C. S. B. Gomes, P. T. Gomes, R. E. Di Paolo, A. L. Maçanita, M. J. Calhorda, A. Charas, J. Morgado and M. T. Duarte, *Dalton Trans.*, 2012, **41**, 8502–8505. Erratum no. 1: *Dalton Trans.*, 2012, **41**, 14713; Erratum no. 2: *Dalton Trans.*, 2013, **42**, 16969; (*b*) M. J. Calhorda, D. Suresh, P. T. Gomes, R. E. Di Paolo and A. L. Maçanita, *Dalton Trans.*, 2012, **41**, 13210–13217; (*c*) D. Suresh, P. S. Lopes, B. Ferreira, C. A. Figueira, C. S. B. Gomes, P. T. Gomes, R. E. Di Paolo, A. L. Maçanita, M. T. Duarte, A. Charas, J. Morgado and M. J. Calhorda, *Chem. – Eur. J.*, 2014, **20**, 4126–4140.

6 D. Suresh, B. Ferreira, P. S. Lopes, C. S. B. Gomes, P. Krishnamoorthy, A. Charas, D. Vila-Viçosa, J. Morgado, M. J. Calhorda, A. L. Maçanita and P. T. Gomes, *Dalton Trans.*, 2016, **45**, 15603–15620.

7 P. Krishnamoorthy, B. Ferreira, C. S. B. Gomes, D. Vila-Viçosa, A. Charas, J. Morgado, M. J. Calhorda, A. L. Maçanita and P. T. Gomes, *Dyes Pigm.*, 2017, **140**, 520–532.

8 D. Suresh, C. S. B. Gomes, P. S. Lopes, C. A. Figueira, B. Ferreira, P. T. Gomes, R. E. Di Paolo, A. L. Maçanita, M. T. Duarte, A. Charas, J. Morgado, D. Vila-Viçosa and M. J. Calhorda, *Chem. – Eur. J.*, 2015, **21**, 9133–9149.

9 A. I. Rodrigues, C. A. Figueira, C. S. B. Gomes, D. Suresh, B. Ferreira, R. E. Di Paolo, D. de Sa Pereira, F. B. Dias, M. J. Calhorda, J. Morgado, A. L. Maçanita and P. T. Gomes, *Dalton Trans.*, 2019, **48**, 13337–13352.

10 (*a*) F. Masetti, U. Mazzucato and G. Galiazzo, *J. Lumin.*, 1971, **4**, 8–12; (*b*) K. N. Solovyov and E. A. Borisevich, *Phys.-Usp.*, 2005, **48**, 231–235; (*c*) H. Morrison and A. Miller, *Tetrahedron*, 1981, **37**, 3405–3409; (*d*) A. Rodriguez-Serrano, V. Rai-Constapel, M. C. Daza, M. Doerr and C. M. Marian, *Phys. Chem. Chem. Phys.*, 2015, **17**, 11350–11358; (*e*) N. Adarsh, R. R. Avirah and D. Ramaiah, *Org. Lett.*, 2010, **12**, 5720–5723; (*f*) A. Karatay, M. C. Miser, X. Cui, B. Küçüköz, H. Yilmaz, G. Sevinç, E. Akhüseyin, X. Wu, M. Hayvali, H. G. Yaglioglu, J. Zhao and A. Elmali, *Dyes Pigm.*, 2015, **122**, 286–294; (*g*) J. Al Anshori, T. Slanina, E. Palao and P. Klán, *Photochem. Photobiol. Sci.*, 2016, **15**, 250–259.

11 D. O. A. Garrido, G. Buldain and B. Frydman, *J. Org. Chem.*, 1984, **49**, 2619–2622.

12 (*a*) T. Tanaka and O. Yamauchi, *Chem. Pharm. Bull.*, 1961, **9**, 588–592; (*b*) R. A. Jones, *Aust. J. Chem.*, 1964, **17**, 894–900; (*c*) K.-N. Yeh and R. H. Barker, *Inorg. Chem.*, 1967, **6**, 830–833; (*d*) A. W. Addison and J. H. Stenhouse, *Inorg. Chem.*, 1978, **17**, 2161–2165; (*e*) Y. Yoshida, S. Matsui, Y. Takagi, M. Mitani, T. Nakano, H. Tanaka, N. Kashiwa and T. Fujita, *Organometallics*, 2001, **20**, 4793–4799; (*f*) S. A. Carabineiro, L. C. Silva, P. T. Gomes, L. C. J. Pereira, L. F. Veiros, S. I. Pascu, M. T. Duarte, S. Namorado and R. T. Henriques, *Inorg. Chem.*, 2007, **46**, 6880–6890; (*g*) P. J. Figiel, A. Sibaouih, J. U. Ahmad, M. Nieger, M. T. Räisänen, M. Leskelä and T. Repo, *Adv. Synth. Catal.*, 2009, **351**, 2625–2632.

13 A. Mohamadou, J. P. Barbier and R. P. Hugel, *Polyhedron*, 1992, **11**, 2697–2702.

14 (*a*) R. K. Sharma and N. Kharasch, *Angew. Chem., Int. Ed.*, 1968, **7**, 36–44; (*b*) Y.-L. Chen, C. Sinha, I.-C. Chen, K.-L. Liu, Y. Chi, J.-K. Yu, P.-T. Chou and T.-H. Lu, *Chem. Commun.*, 2003, 3046–3047.

15 E. Pomarico, P. Pospíšil, M. E. F. Bouduban, J. Vestfrid, Z. Gross, S. Záliš, M. Chergui and A. Vlček, *J. Phys. Chem. A*, 2018, **122**, 7256–7266.

16 C. Murawski, K. Leo and M. C. Gather, *Adv. Mater.*, 2013, **25**, 6801–6827.

17 G. M. Sheldrick, *SADABS, Program for Empirical Absorption Correction*, University of Göttingen, Göttingen, Germany, 1996.

18 M. C. Burla, R. Caliandro, M. Camalli, B. Carrozzini, G. L. Cascarano, L. De Caro, C. Giacovazzo, G. Polidori and R. Spagna, *J. Appl. Crystallogr.*, 2005, **38**, 381–388.

19 M. C. Burla, R. Caliandro, B. Carrozzini, G. L. Cascarano, C. Cuocci, C. Giacovazzo, M. Mallamo, A. Mazzone and G. Polidori, *J. Appl. Crystallogr.*, 2015, **48**, 306–309.
20 (*a*) SHELXL: G. M. Sheldrick, *Acta Crystallogr., Sect. C: Struct. Chem.*, 2015, **71**, 3–8; (*b*) C. B. Hübschle, G. M. Sheldrick and B. Dittrich, ShelXle: a Qt graphical user interface for SHELXL, *J. Appl. Crystallogr.*, 2011, **44**, 1281–1284.
21 L. J. Farrugia, *J. Appl. Crystallogr.*, 2012, **45**, 849–854.
22 B. Ferreira, P. F. Silva, J. S. Seixas de Melo, J. Pina and A. L. Maçanita, *J. Phys. Chem. B*, 2012, **116**, 2347–2355.
23 G. Stricker, in *Effective implementation of modulation functions in deconvolution and reconvolution of analytical signals*, ed. M. Bouchy, University Press, Nancy, France, 1982.
24 See: http://www.zeon.co.jp/business_e/enterprise/speplast/speplast1.
25 For more experimental details see: P. Pander, P. Data and F. B. Dias, *J. Visualized Exp.*, 2018, (142), e56614, DOI: 10.3791/56614.
26 J. C. de Mello, H. F. Wittmann and R. H. Friend, *Adv. Mater.*, 1997, **9**, 230–232.
27 I. Carmichael and G. L. Hug, *J. Phys. Chem. Ref. Data*, 1986, **15**, 1.
28 G. te Velde, F. M. Bickelhaupt, E. J. Baerends, C. F. Guerra, S. J. van Gisbergen, G. J. Snijders and T. Ziegler, *J. Comput. Chem.*, 2001, **22**, 931–967.
29 C. F. Guerra, J. G. Snijders, G. te Velde and E. J. Baerends, *Theor. Chem. Acc.*, 1998, **99**, 391–403.
30 Theoretical Chemistry, Vrije Universiteit, Amsterdam, TN, ADF2013 SCM http://www.scm.com (last: accessed October 2019).
31 R. G. Parr and W. Yang, *Density-Functional Theory of Atoms and Molecules*, Oxford University Press, 1989.
32 S. H. Vosko, L. Wilk and M. Nusair, *Can. J. Phys.*, 1980, **58**, 1200–1211.
33 M. Ernzerhof and G. Scuseria, *J. Chem. Phys.*, 1999, **110**, 5029–5036.
34 C. Adamo and V. Barone, *J. Chem. Phys.*, 1999, **110**, 6158–6170.
35 F. Wang and T. Ziegler, *J. Chem. Phys.*, 2005, **123**, 154102.
36 E. van Lenthe, A. Ehlers and E.-J. Baerends, *J. Chem. Phys.*, 1999, **110**, 8943–8953.
37 S. J. A. van Gisbergen, A. Rosa, G. Ricciardi and E. J. Baerends, *J. Chem. Phys.*, 1999, **111**, 2499–2506.
38 A. Rosa, E. J. Baerends, S. J. A. van Gisbergen, E. van Lenthe, J. A. Groeneveld and J. G. Snijders, *J. Am. Chem. Soc.*, 1999, **121**, 10356–10365.
39 S. J. A. van Gisbergen, J. A. Groeneveld, A. Rosa, J. G. Snijders and E. J. Baerends, *J. Phys. Chem. A*, 1999, **103**, 6835–6844.
40 J. Moussa, L.-M. Chamoreau, A. D. Esposti, M. P. Gullo, A. Barbieri and H. Amouri, *Inorg. Chem.*, 2014, **53**, 6624–6633.
41 S. Hirata and M. Head-Gordon, *Chem. Phys. Lett.*, 1999, **314**, 291–299.
42 M. Reiher, O. Salomon and B. A. Hess, *Theor. Chem. Acc.*, 2001, **107**, 48–55.
43 S. Grimme, *J. Comput. Chem.*, 2004, **25**, 1463–1473.
44 A. D. Becke, *J. Chem. Phys.*, 1998, **109**, 2092–2098.
45 J. P. Perdew, *Phys. Rev. B: Condens. Matter Mater. Phys.*, 1986, **33**, 8822–8824.
46 J. P. Perdew, Erratum, *Phys. Rev. B: Condens. Matter Mater. Phys.*, 1986, **34**, 7406–7406.
47 J. Morgado, A. Charas, J. A. Fernandes, I. S. Gonçalves, L. D. Carlos and L. Alcácer, *J. Phys. D: Appl. Phys.*, 2006, **39**, 3582–3587.